

**AEDC-TR-69-49**

**ARCHIVE COPY  
DO NOT LOAN**

*cy*

*I-516*



**COMPARISON OF EXPERIMENTAL AND PREDICTED  
AXIAL PRESSURE VARIATION FOR METALLIC TARGETS  
IMPACTED BY METALLIC SPHERES**

**James P. Billingsley**

**ARO, Inc.**

PROPERTY OF U. S. AIR FORCE  
AEDC LIBRARY  
F40600-69-C-0001

**July 1969**

This document has been approved for public release  
and sale; its distribution is unlimited.

**VON KÁRMÁN GAS DYNAMICS FACILITY  
ARNOLD ENGINEERING DEVELOPMENT CENTER  
AIR FORCE SYSTEMS COMMAND  
ARNOLD AIR FORCE STATION, TENNESSEE**

AEDC TECHNICAL LIBRARY



0574 9E000 0220 5 0720 0036 7450

PROPERTY OF U. S. AIR FORCE  
AEDC LIBRARY  
F40600 - 69 - C - 0001

# ***NOTICES***

When U. S. Government drawings specifications, or other data are used for any purpose other than a definitely related Government procurement operation, the Government thereby incurs no responsibility nor any obligation whatsoever, and the fact that the Government may have formulated, furnished, or in any way supplied the said drawings, specifications, or other data, is not to be regarded by implication or otherwise, or in any manner licensing the holder or any other person or corporation, or conveying any rights or permission to manufacture, use, or sell any patented invention that may in any way be related thereto.

Qualified users may obtain copies of this report from the Defense Documentation Center.

References to named commercial products in this report are not to be considered in any sense as an endorsement of the product by the United States Air Force or the Government.

COMPARISON OF EXPERIMENTAL AND PREDICTED  
AXIAL PRESSURE VARIATION FOR METALLIC TARGETS  
IMPACTED BY METALLIC SPHERES

James P. Billingsley  
ARO, Inc.

This document has been approved for public release  
and sale; its distribution is unlimited.

## FOREWORD

The work reported herein was sponsored by Headquarters, Arnold Engineering Development Center (AEDC), under Program Element 65401F.

The results of research presented were obtained by ARO, Inc. (a subsidiary of Sverdrup & Parcel and Associates, Inc.), contract operator of AEDC, Air Force Systems Command, (AFSC), Arnold Air Force Station, Tennessee, under Contract F40600-69-C-0001. The research was conducted from November 27, 1967, to June 30, 1968, under ARO Project No. VS2856, and the manuscript was submitted for publication on January 31, 1969.

The author wishes to acknowledge the help received from various ARO, Inc., employees. Without the assistance of the VKF Hypervelocity Impact Range technicians, craftsmen, and supervisory personnel, this report would not be possible. Mr. W. C. Armstrong, MD/CCO, has aided the author in obtaining the numerical results presented herein.

This technical report has been reviewed and is approved.

Marshall K. Kingery  
Research Division  
Directorate of Plans  
and Technology

Edward R. Feicht  
Colonel, USAF  
Director of Plans  
and Technology

**ABSTRACT**

Sufficient experimental data have been collected for five different cases of high velocity metallic impact so that the axial shock pressure variation can be traced in a semi-infinite target. The metals utilized were aluminum alloys and copper. In all cases, a spherical projectile was fired into a target plate of similar material. The aft spall velocity of the target plate was measured by means of a high-speed framing camera, and the shock pressure at the axial location in a semi-infinite target corresponding to the target plate thickness was computed from this spall velocity. These data are compared with the results of various theoretical methods for predicting the shock pressure variation in semi-infinite targets. The present data are also compared with other available experimental data.

## CONTENTS

	<u>Page</u>
ABSTRACT. . . . .	iii
NOMENCLATURE. . . . .	vi
I. INTRODUCTION . . . . .	1
II. EXPERIMENTAL PROCEDURE	
2.1 Basic Principles . . . . .	2
2.2 Instrumentation and Measurement . . . . .	3
III. DISCUSSION OF CERTAIN METHODS FOR PRE- DICTING HYPERVELOCITY IMPACT SHOCK PHENOMENA	
3.1 OIL, a Numerical Computer Code . . . . .	4
3.2 Quasi-Steady Blast Wave Analysis . . . . .	5
3.3 PEAK, Semi-Empirical Analysis . . . . .	6
3.4 GM/DRL's Empirical Relation . . . . .	7
IV. RESULTS AND DISCUSSION	
4.1 Comparison of Theory and Experiment . . . . .	8
4.2 Material Strength Effects . . . . .	10
4.3 Hypervelocity Impact Scaling and Similarity . . . . .	11
V. CONCLUSIONS AND RECOMMENDATIONS . . . . .	13
REFERENCES . . . . .	13

## APPENDIXES

## I. ILLUSTRATIONS

Figure

1. Plane Shock Geometry . . . . .	19
2. Simplified Hemispherical Shock Geometry . . . . .	20
3. Beckman & Whitley High-Speed Framing Camera Sequential Photographs for Shot PI-13 . . . . .	21
4. Comparison of Experimental and Theoretical Pressure Data for Case A1-1 . . . . .	22
5. Comparison of Experimental and Theoretical Pressure Data for Case A1-2 . . . . .	23
6. Comparison of Experimental and Theoretical Pressure Data for Case A1-3 . . . . .	24
7. Comparison of Experimental and Theoretical Pressure Data for Case A1-4 . . . . .	25

<u>Figure</u>		<u>Page</u>
8.	Comparison of Experimental and Theoretical Pressure Data for Case Cu-1. . . . .	26
9.	Comparison of Experimental and Theoretical Particle Velocity for Case Al-1 . . . . .	27
10.	Comparison of Experimental and Theoretical Particle Velocity for Case Al-2 . . . . .	28
11.	Comparison of Experimental and Theoretical Particle Velocity for Case Al-3 . . . . .	29
12.	Comparison of Experimental and Theoretical Particle Velocity for Case Al-4 . . . . .	30
13.	Comparison of Experimental and Theoretical Particle Velocity for Case Cu-1 . . . . .	31
14.	Normalized Results for Condition Al-1, Al-2, and Cu-3. . . . .	32
15.	Normalized Results for Condition Al-1, Al-2, Al-3, and Al-4 . . . . .	33
II.	HYDRODYNAMIC OIL CODE PREDICTIONS . . . . .	34
III.	TABULATION OF EXPERIMENTAL DATA . . . . .	41
IV.	NAVAL ORDNANCE LABORATORY EXPERIMENTAL DATA . . . . .	47
V.	TARGET MATERIAL YIELD STRENGTH . . . . .	49

## NOMENCLATURE

A	Constant defined by Eq. (8), km/sec
C	Elastic wave velocity in a slender rod, $\sqrt{E/\rho_0}$ , km/sec
C <sub>1</sub>	Constant defined by Eq. (10)
C <sub>H</sub>	Velocity of the rarefaction wave from the edge of the target projectile interface, km/sec (see Ref. 2, p. 84)
C <sub>0</sub>	Constant in Eq. (5) which is similar to the elastic wave velocity in a slender rod, km/sec
d	Diameter of spherical projectile, cm
E	Young's Modulus, kb (1 kb is 14,504 lb/in. <sup>2</sup> )

$E_t$	Kinetic energy of the projectile, ergs
$I_o$	Internal energy per unit mass before shock front passage, ergs/gm or $\text{cm}^2/\text{sec}^2$
$I_s$	Internal energy per unit mass immediately after shock front passage, ergs/gm or $\text{cm}^2/\text{sec}^2$
$K$	Quantity defined by Eq. (9)
$L_p$	Length of cylindrical projectile in the OIL code, cm
$L_T$	Length of cylindrical target in the OIL code, cm
$M_p$	Mass of projectile, gm
$P_o$	Initial pressure before shock front passage, kb
$P_s$	Pressure immediately behind the shock front, kb
$R$	Radial position of the shock front in spherical coordinates measured from point of initial projectile contact, cm
$R_o$	Reference length for impact and explosion phenomena defined by Eq. (15), cm
$R_T$	Radius of cylindrical target in the OIL code, cm
$S$	Constant in Eq. (5), dimensionless
$T$	Target thickness, cm
$t_1$	Quantity defined by Eq. (11), sec
$U_{FS}$	Free-surface velocity caused by reflected shock front, km/sec
$U_p$	Material particle velocity behind an advancing shock front relative to undisturbed material ahead of the front, km/sec
$U'_p$	Material particle velocity behind a reflected shock front relative to the material ahead of the wave, km/sec
$U_s$	Shock front propagation velocity relative to undisturbed material ahead of the front, km/sec
$U'_s$	Reflected shock propagation velocity relative to the material ahead of the reflected front, km/sec
$U_{s\text{max}}$	Maximum shock propagation velocity which occurs at the initial moment of projectile-target contact, km/sec
$V_I$	Projectile impact velocity, km/sec
$X$	Radial position in cylindrical coordinates for the OIL code, cm (see Fig. II-1)

Y	Axial position in cylindrical coordinates for the OIL code, cm (see Fig. II-1)
Z	Axial position along the axis of symmetry in the target measured from the point of initial projectile-target contact, cm (see Fig. 2)
$Z_1$	Quantity defined by Eq. (12)
$Z_0$	Quantity defined by Eq. (13)
$\bar{\alpha}$	Constant = 0.368 (Eq. (9))
$\gamma$	Poly tropic exponent in the relation $P/\rho^\gamma = \text{constant}$
$\rho_0$	Mass density of undisturbed material ahead of shock front, gm/cm <sup>3</sup>
$\rho_s$	Mass density of material immediately behind the shock front, gm/cm <sup>3</sup>

## SECTION I INTRODUCTION

Technology advances associated with the ballistic missile and space programs have created a new area of research known as the hypervelocity impact problem. Hypervelocity impact may be roughly defined as impact of two objects with a relative velocity greater than the velocity of elastic wave propagation in the materials under consideration. For many of the commonly used structural metals, the velocity of elastic wave propagation is approximately 5.0 km/sec (16,400 ft/sec). Regardless of the magnitude of impact velocity, a knowledge of material behavior under highly transient loading conditions is essential to properly predict the damage potential of a given collision. Somewhat similar conditions of highly transient impact loads also may be caused by explosive detonation, shaped charge metallic jet penetration, and high energy forming processes. The shock wave which advances into the target is a phenomenon which is common to these impact conditions.

There is a dearth of experimental data concerning shock propagation phenomena in semi-infinite targets struck by small, high velocity projectiles. Experimental data are essential to properly evaluate the usefulness and versatility of numerical and analytical schemes available to predict impact shock variables. Consequently, there were two primary objectives of the present investigation. These were:

1. To obtain experimental shock pressure data for various conditions of metallic solid impact so that the shock pressure variation with propagation distance could be traced, and
2. To compare the experimental pressure data variation with certain theoretical and empirical predictions.

These objectives have been accomplished for five conditions wherein spherical projectiles were impacted into plates of similar material having various thicknesses. These conditions are listed below:

<u>Case</u>	<u>V<sub>I</sub>, km/sec</u>	<u>V<sub>I</sub>, ft/sec</u>	<u>d<sub>p</sub>, cm</u>	<u>d<sub>p</sub>, in.</u>	<u>Projectile Material</u>	<u>Target Material</u>
A1-1	7.32	24,000	0.476	0.1875	2017 Al	6061-T6 Al
A1-2	7.63	25,000	0.635	0.2500	2017 Al	6061-T6 Al
A1-3	4.42	14,500	0.635	0.2500	2017 Al	6061-T6 Al
A1-4	1.52	5,000	0.635	0.2500	2017 Al	2024-0 Al
Cu-1	6.10	20,000	0.476	0.1875	Copper	Copper

The present experimental data were obtained from tests conducted in the hypervelocity impact ranges (Armament Test Cell, Hyperballistic, (S1) and (S2)) of the Aeroballistics Branch, von Kármán Gas Dynamics Facility (VKF). A description of these facilities is contained in Ref. 1.

## SECTION II EXPERIMENTAL PROCEDURE

### 2.1 BASIC PRINCIPLES

When a projectile such as a sphere or cylindrical slug impacts a semi-infinite target, an essentially plane shock wave exists in both the projectile and the target for a very short time after initial contact. The pressure behind these initial one-dimensional shock fronts is the largest pressure that occurs during the impact process. This one-dimensional condition persists until the front has propagated approximately one projectile radius into the target. By then, rarefaction (tensile) waves from the edge of the projectile at the projectile-target interface have reached the axis of symmetry (Refs. 2 and 3). The effect of these rarefaction waves is to diminish the strength of the shock and to alter its shape from a plane front to an approximately hemispherical front. The shock continues to decrease in strength because of spherical attenuation and additional rarefaction waves.

At each point on this hemispherical shock front, it is assumed that the one-dimensional Rankine-Hugoniot conditions still apply. Considerable justification for this assumption is contained in Ref. 4. The Rankine-Hugoniot relations are:

$$\frac{\rho_s}{\rho_0} = \frac{U_s}{U_s - U_p} \quad (1)$$

$$P_s - P_0 = \rho_0 U_s U_p \approx P_s \quad (2)$$

$$I_s - I_0 = \left( \frac{P_s + P_0}{2} \right) (1/\rho_0 - 1/\rho_s) \quad (3)$$

The initial pressure,  $P_0$ , is generally so small that it can be neglected in comparison with the shock pressure,  $P_s$ . If the shock velocity,  $U_s$ , and the particle velocity,  $U_p$ , are known at a point on the shock front, the shock pressure may be computed from Eq. (2).

Figure 1 (Appendix I) is a schematic of a plane shock front before and after a normal reflection from the unsupported aft surface (free surface). It has been shown analytically (Ref. 5) that the free-surface

velocity,  $U_{FS}$ , is twice the particle velocity,  $U_p$ , to a high degree of accuracy. That is:

$$U_{FS} = 2 U_p \quad (4)$$

Experimental data reveal that the shock velocity is a linear function of particle velocity for many materials, viz:

$$U_s = C_0 + S U_p \quad (5)$$

The constants  $C_0$  and  $S$  may be found in Refs. 6 and 7 for aluminum and copper. The following constants for Eq. (5) were used in the present investigation:

<u>Material</u>	<u><math>C_0</math>, km/sec</u>	<u><math>S</math></u>
Aluminum	5.345	1.373
Copper	3.958	1.497

Thus, if the free-surface velocity is measured at a point, the shock pressure can be computed from Eqs. (2), (4), and (5).

Investigators at General Motors Defense Research Laboratory (GM/DRL) (Ref. 8) have applied the above analysis to plates which were impacted by spherical projectiles. This configuration is shown schematically in Fig. 2. The hemispherical shock front is parallel to the aft surface in a small region near the axis of symmetry. A high-speed framing camera was used to measure the velocity of the aft surface,  $U_{FS}$ , along the centerline during the initial motion. The pressure at the axial position corresponding to the plate thickness was computed by the procedure mentioned above. Similar tests with the same impact conditions, but with different target thicknesses, allowed the shock pressure to be determined as a function of axial position (or shock front radius). A similar procedure was utilized in the present investigation.

## 2.2 INSTRUMENTATION AND MEASUREMENT

The basic instrument used to measure the target aft surface velocity was a Beckman & Whitley (B&W) Model 192 high-speed framing camera. Figure 3 contains sequential photographs taken by the B&W camera for a typical data shot.

In order to obtain the target spallation velocities, individual photographs were enlarged, and travel distances and grid lines were scaled off. These data, in conjunction with the framing rate and optical constants, were sufficient to determine  $U_{FS}$ . The data collected for very thin targets and very thick targets are not considered as accurate as the data for moderately thick targets. For thin targets, there were usually only two or three frames which showed initial surface motion. The free-surface motion per frame was small for thick targets. It is estimated that the magnitude of a given data point is within 10 percent of the true value. Consequently, to establish a data trend, it was desirable to collect multiple data points for each specific target thickness.

The projectile velocity was determined from the B&W film records. Also for the majority of the data shots, the projectile velocity was measured by a shadowgraph system which is described in Ref. 1. The projectile velocity data from the shadowgraph and from the B&W camera show an average discrepancy of less than 3 percent.

### SECTION III

#### DISCUSSION OF CERTAIN METHODS FOR PREDICTING HYPERVELOCITY IMPACT SHOCK PHENOMENA

Even though experimental data for impact shock phenomena in metals are scarce, there is no lack of theoretical or empirical methods to predict these phenomena. These methods range from highly complex numerical schemes to simple empirical formulas. Even so, most of these analyses lean rather heavily on the one-dimensional data of Refs. 5, 6, and 7. The following review is by no means a comprehensive discussion of all the analyses available. No attempt has been made to modify any of the following analyses in order to provide better agreement with the present data.

#### 3.1 OIL, A NUMERICAL COMPUTER CODE

References 9 and 10 contain a Fortran listing of the OIL computer code as developed by General Atomic personnel. This program has the capability of treating the case of a right-circular cylinder impacting a semi-infinite target, which is also a right-circular cylinder. Both target and projectile must be of similar materials. Basically, the OIL program numerically solves the inviscid two-dimensional equations of

fluid mechanics in conjunction with an equation of state that is suitable for solids. This is a so-called "hydrodynamic" code since material strength effects are not taken into account.

References 11 and 12 contain detailed discussions of the results obtained from the OIL hydrodynamic code and other similar codes. One of the more significant results, so far as the present investigation is concerned, was that spherical and right-circular projectiles of equal mass gave similar results, particularly during the latter stages of shock decay. According to Ref. 12, "Substantial differences are limited to the very early times in which the projectile is embedding itself in the target plate." Consequently, the spherical projectiles used in the present experiments were simulated in the OIL code by a right-circular cylinder ( $L_p = 2R_p$ ) of equal volume.

Table II-1 (Appendix II) contains the pertinent dimensions of the targets and projectiles used in the OIL code computations. Figure II-1 is a sketch of the target and projectile radial cross section grid, which was utilized for all cases. The constants controlling the time step,  $\Delta t$ , were  $FFA = 0.50$  and  $FFB = 0.10$ . It is to be noted that the magnitudes of the shock pressures computed by OIL were somewhat dependent on the grid size and time step constants.\* For this reason, the results from this complex numerical code should be used with caution, even though they are very valuable contributions to the understanding of hypervelocity impact phenomena.

All computations were made on the AEDC Central Computer Operations IBM 360/50 machine. The results are tabulated in Appendix II.

### 3.2 QUASI-STEADY BLAST WAVE ANALYSIS

The blast wave analysis was originally formulated to solve the problem of an intense explosion in a gas (Refs. 13 and 14). Several investigators have applied the blast wave analysis to the hypervelocity impact problem and the explosive blast problem in solids (Refs. 15, 16, and 17). In these applications, it was assumed that the shocked solid obeys a relation analogous to the polytropic gas law,  $P/\rho^\gamma = \text{constant}$ . The exponent  $\gamma$  was determined from the Rankine-Hugoniot pressure-volume data of Refs. 5, 6, and 7. These constant  $\gamma$  solutions match

---

\*This dependence has received little, if any, attention in previous reports describing OIL.

all the Rankine-Hugoniot shock conditions at only one point. In particular, the density is the same for all values of the shock pressure, i. e. ,

$$\rho_s = \left( \frac{\gamma + 1}{\gamma - 1} \right) \rho_o = \text{constant}$$

In an attempt to improve the basic blast wave method for solids, Kirchner and Rae (Ref. 17) have developed an analysis for solids, which is somewhat analogous to Ōshima's quasi-similarity solution for gases (Ref. 18). They used  $\gamma$  as a variable parameter to match the Rankine-Hugoniot conditions (Eqs. (1), (2), and (3)) at each point of the decaying shock front. The experimentally derived linear relation between the shock and particle velocities (Eq. (5)) was utilized as an approximation to the equation of state (a so-called "C<sub>0</sub>-S material"). Rae has presented nondimensional results for his "quasi-steady" analysis in Ref. 19. These data allow a rapid computation of the shock pressure variation to be made for any material whose C<sub>0</sub>-S constants are known.

### 3.3 PEAK, SEMI-EMPIRICAL ANALYSIS

Heyda and Riney have developed a semi-empirical relation to predict the axial variation of the maximum shock pressure caused by hyper-velocity impact (Refs. 2 and 3). The following relation for the shock velocity,  $\dot{Z}$ , as a function of axial position,  $Z$ , was derived by heuristic reasoning in Ref. 20:

$$U_s = \dot{Z} = 4 A K \left[ \frac{1}{\sqrt{Z - Z_o}} - \frac{K}{Z - Z_o} \right] \quad (6)$$

This was integrated to give the shock arrival time as a function of position:

$$\begin{aligned} 2 A K t = & (1/3)(Z - Z_o)^{3/2} + (K/2)(Z - Z_o) \\ & + K^2 (Z - Z_o)^{1/2} + K_3 \ln (\sqrt{Z - Z_o} - K) \\ & + C_1 \end{aligned} \quad (7)$$

where the constants  $A$ ,  $K$ , and  $C_1$  are given by

$$A = 1.055 U_{s_{max}} \quad (8)$$

$$K = \bar{\alpha} (R_p^2 L_p)^{1/6} (V_I/C_o)^{-1/3} \quad (9)$$

$$C_1 = 2 A K t_1 - K^3 [6.67 + \ln (1.59 K)] \quad (10)$$

and where

$$\bar{a} = 0.368$$

$$t_1 = \frac{L_p}{\sqrt{C_H^2 - (U_{s_{max}} - V_1/2)^2}} \quad (11)$$

$$(12)$$

$$Z_1 = U_{s_{max}} t_1$$

$$Z_0 = Z_1 - 6.717 K^2 \quad (13)$$

$C_H$  = Velocity of the rarefaction wave from the edge of the target projectile interface,  $\sqrt{\partial P / \partial \rho}$ . This is computed from the equation of state for tensile stresses.

The constants were determined from the boundary conditions and/or numerical results of the PICWICK code (Refs. 21 and 22) for hyper-velocity impact. Consequently, the above relations match the PICWICK results quite closely for shock pressure variation along the central axis (strictly for hypervelocity impact conditions).

### 3.4 GM/DRL'S EMPIRICAL RELATION

Investigators at GM/DRL (Ref. 8) have proposed the following empirical relation for the maximum shock pressure variation in an aluminum target undergoing hypervelocity impact:

$$P_s = \frac{1.243 \cdot P_{s_{max}}}{(R/R_p)^{1.6}} \quad (14)$$

$$R > 1.14 \cdot R_p$$

where  $R_p$  is the spherical projectile radius and  $P_{s_{max}}$  is the maximum shock pressure that occurs when initial contact is made.

The above relation was determined for targets and projectiles of 1100-0 aluminum under conditions similar to case Al-1 as described previously. For pressures from 1 megabar (mb) to 300 kilobars, it was recommended that 1.8 be used for the distance exponent instead of 1.6. Actually, the distance exponent varies continually and is approximately 1.0 when elastic conditions exist. The exponent value of 1.6 was used in the present work.

## SECTION IV RESULTS AND DISCUSSION

### 4.1 COMPARISON OF THEORY AND EXPERIMENT

The experimental data obtained in this investigation are tabulated in Appendix III. These data are also presented graphically in Figs. 4 through 15, where they are compared with theoretical and empirical predictions and other experimental data.

Data for the maximum shock pressure variation along the axial centerline of the target are shown in Figs. 4 through 8. The present data were computed from the measured aft surface velocities as discussed previously. Figure 4 also contains the experimental data of Ref. 8. Reference 8 data and the present data have somewhat different trends and magnitudes in the transition region between high and low pressure (100 to 300 kb). This is believed to be a material strength effect and is discussed later.

Reference 23 contains experimental data for hypervelocity-impact-generated shock pressures in a thick target (see Appendix IV, Table IV-1, and Fig. IV-1). Figure IV-1 was utilized to extrapolate the Naval Ordnance Laboratory (NOL) data to the Case A1-2 impact velocity, and this extrapolated point is shown in Fig. 5. It is evident from Figs. 5 and IV-1 that this extrapolated point is about 50 percent greater in magnitude than the present results for Case A1-2. Although a portion of this difference can be attributed to data scatter, it is believed that material solid strength effects also contribute significantly to this discrepancy. Figure 6 contains one data point from Ref. 23 and the present data for Case A1-3. This point agrees with the trend of the present data, although a strict quantitative comparison based on extrapolating the present data is not feasible.

In general, the OIL predictions are in fair agreement with the present results for conditions A1-1 and A1-2, particularly in the high pressure region of shock decay. The present data have a somewhat different trend and magnitude in the transition region between high and low pressures (see Figs. 4 and 5). For Case A1-3 (Fig. 6), the hydrodynamic OIL results agree very well with the low pressure data ( $P_s < 100$  kb) diverge somewhat from the data at intermediate pressures. The favorable comparison at low pressures was unexpected since material strength effects were not included in the computations.

The GM/DRL empirical formula for the shock pressure-distance variation agrees very well with the OIL prediction for Cases A1-1 and A1-2. For Case A1-3, the GM/DRL formula agrees very well with the

experimental low pressure data but predicts somewhat larger pressures than were experimentally obtained in the initial stage of shock decay. Case Al-3 has a somewhat lower impact velocity than the condition under which the constants in Eq. (14) were derived.

The PEAK predictions for shock pressure are somewhat greater than the experimental data in the initial stage of shock pressure decay. This could be remedied by changing one or more of the empirical constants. The PEAK trend follows the experimental data trend in the high pressure region but deviates greatly from the data in the transition and low pressure region. Since PEAK closely matches the PICWICK results (Ref. 2), it follows that the above comments would also apply to PICWICK. However, PICWICK has provisions for material strength effects. A judicious selection of strength parameters in PICWICK could possibly improve the agreement, particularly in the transitional and low pressure regimes.

The quasi-steady blast wave analysis compares rather favorably with the present data in the low pressure regime for the Al-1, Al-2, and Al-3 conditions. For Cases Al-1 and Al-2, the quasi-steady blast wave analysis underestimates the pressures in the transition regime (100 to 300 kb) and overestimates the pressures in the initial stage of pressure decrease. This behavior indicates that somewhat better initial agreement might be obtained from further modifications and extensions of the blast wave analysis as published by Bach and Lee (Ref. 24) and Whitesides (Ref. 25).

For Case Al-4 (Fig. 7), OIL, PEAK, quasi-steady blast wave analysis, and the GM/DRL empirical relation all have the same trends as for the other aluminum impact conditions with larger impact velocity. However, all methods grossly overestimate the magnitude of the present data, both in the initial and final stages of shock propagation. This is not entirely unexpected since the theoretical schemes are based primarily on hydrodynamic assumptions with no material strength effects. As discussed later, one effect of material strength at relatively low pressures is to attenuate the shock strength more rapidly than would be expected on the basis of hydrodynamic theory.

In general, the theoretical and experimental results for Case Cu-1 (Fig. 8) do not compare as favorably as might be expected. In particular, the experimental pressures are considerably higher than the OIL code prediction, except for data obtained from very thin targets.

Figures 9 through 13 contain the present experimental particle velocity data ( $U_{FS}/2$ ) as a function of axial velocity,  $Z$ . The particle velocity is a more fundamental quantity than the pressure since fewer assumptions are required to obtain it from the basic  $U_{FS}$  measurement. The particle velocity predictions from the OIL hydrodynamic code are also shown in Figs. 9 through 13. The experimental data-OIL prediction trends are much the same as those for the shock pressure comparison. Thus, many of the previous comments concerning the shock pressure trends are applicable to the particle velocity comparisons also.

#### 4.2 MATERIAL STRENGTH EFFECTS

Based on a theoretical study, Mok (Ref. 26) stated that the effects of solid strength become important when the shock pressure has decreased to within two orders of magnitude of the yield stress of the material. Mok's investigation revealed that the effect of material strength is to attenuate the shock pressure more rapidly than a hydrodynamic analysis would predict. Some evidence of this effect for wax is contained in Ref. 27. This trend is also exhibited by the present data for Case A1-4 when compared with the hydrodynamic OIL code predictions (Fig. 7), in that the data have a lower magnitude than the OIL results. It should be pointed out that these data were taken for a rather low impact velocity where OIL results may not be applicable.

According to Mok (Ref. 26), increasing the yield strength will also increase the maximum shock pressure attenuation in the low pressure region. Experimental evidence for this trend is displayed in Ref. 23. There is some indication of this effect in the low pressure ( $P_S < 100$  kb) results for Case A1-2. It was previously mentioned in Section 4.1 that the A1-2 6061-T6 data have a lower magnitude than the extrapolated point from Ref. 23 for 7075-0. This trend agrees with the above statements concerning shock pressure decay since 6061-T6 has a higher yield strength than 7075-0 (see Appendix V).

Under hypervelocity impact conditions, another trend is exhibited by the present data, particularly in the transition region between high and low pressures (usually 100 to 300 kb). The present shock pressure data for Case A1-1 (6061-T6 aluminum) have a greater magnitude than the Ref. 8 experimental data for 1100-0 aluminum in this transition region. Reference 8 data for pure annealed aluminum compare favorably with the OIL hydrodynamic prediction as shown in Fig. 4. The reason for the discrepancy between the present data and the OIL results (and also the data of Ref. 8) in the transition region is not known. The major difference in the experiments of Ref. 8 and the present experiments

is the target material, but it is not clear why the higher strength targets should experience higher pressure in the transition region. The present pressure data for Case Al-2 in the transition region also have a greater magnitude than is predicted by OIL (Fig. 5). This is consistent with the trend exhibited by the Al-1 data and the OIL prediction.

For Case Cu-1, the thick targets ( $T \geq 1.27$  cm) were soft, high purity copper, and the thin targets were hard, high purity copper. The soft targets were essentially in the annealed condition. As noted previously, the experimental pressures are considerably greater in magnitude than the hydrodynamic OIL code prediction, except for data obtained from the very thin targets. The effects of material strength cannot be evaluated because of insufficient experimental data for soft and hard targets.

#### 4.3 HYPERVELOCITY IMPACT SCALING AND SIMILARITY

As a result of analytical and numerical investigations, a similarity concept has gradually evolved for scaling hypervelocity impact phenomena. This concept has become known as "late stage equivalence." Late stage refers to a period of time (or location) when (or where) the details of projectile construction do not influence the terminal effects of the collision. That is, the projectile shape effects are localized near the point of initial contact, and the projectile effect can be considered essentially as a point source of energy. As the impact velocity increases, projectile shape becomes of less importance.

The late stage equivalence concept as developed from blast wave theory indicates that late stage hypervelocity impact phenomena are similar provided the projectile kinetic energies are the same. For example, if  $M_p V_I^2$  is constant for two hypervelocity impact conditions for aluminum, then projectiles of different size and impact velocity will create the same shock pressure at a remote interior point of the target. This is called energy equivalent scaling. Also, if the remote interior location is fixed and the projectile kinetic energy is varied, then the maximum shock pressure at the point will vary according to the projectile energy. This effect is demonstrated by results from Ref. 23 (see Fig. IV-1, Appendix IV).

It has also been established from numerical studies (Refs. 12 and 28) that the projectile kinetic energy is indeed a dominating scaling factor, with projectile momentum being of secondary importance. As such, the scaling factor is  $M_p V_I^{3\alpha}$  where  $\alpha \approx 0.59$  (Refs. 12 and 28). For strict energy equivalence,  $\alpha = 2/3$ , and for momentum scaling,  $\alpha = 1/3$ . Thus,  $\alpha$  is a measure of the relative importance of energy and momentum for similarity purposes.

According to Refs. 17 and 29, if the projectile kinetic energy is of primary importance, then the characteristic scaling length is:

$$R_o = \left( \frac{E_t}{2\pi \rho_o C_o^2} \right)^{1/3} \quad (15)$$

where  $\rho_o C_o^2$  is a characteristic pressure of hypervelocity impact, and  $C_o$  is the initial wave speed (Eq. (5)). Thus, the radial shock front position,  $R$ , is normalized by  $R_o$ , and shock pressure is normalized by  $\rho_o C_o^2$ . Pertinent scaling information for the present data is listed below:

Case	$M_p$ , gm	$1/2 M_p V_I^2 \times 10^{-10}$ , ergs	$M_p V_I^{3\alpha} \times 10^{-10}$ , $\alpha = 0.59$	$R_o$ , cm	$\rho_o C_o^2$ , kb
Al-1	0.1525	4.085	0.3666	0.2037	773
Al-2	0.3620	10.537	0.9353	0.2784	773
Al-3	0.3620	3.503	0.3558	0.1934	773
Al-4	0.3620	0.418	0.0537	0.0951	773
Cu-1	0.5026	9.350	0.8756	0.2200	1394

The present data in normalized form are graphically presented in Figs. 14 and 15. Figure 14 contains theoretical and experimental results for Cases Al-1, Al-2, and Cu-1. These cases are conditions where hypervelocity scaling theory should apply. Indeed, the normalized experimental data are correlated well enough to provide some justification for hypervelocity impact scaling theory. However, these data show a definite trend which is different from the predicted variation. This is the same trend that was exhibited in each individual case on the linear plots and is believed to be caused by nonhydrodynamic effects at medium and low pressures as discussed earlier.

Figure 15 contains the normalized data for Cases Al-1, Al-2, Al-3, and Al-4. The impact velocity effect on the OIL predictions and the experimental data is very pronounced. Cases Al-3 and Al-4 do not correlate with each other or with cases Al-1 and Al-2. That is, for  $V_I < C$ , the normalized data do not group around a single line, and hypervelocity scaling theory does not apply.

## SECTION V

### CONCLUSIONS AND RECOMMENDATIONS

In general, the present hypervelocity impact data for aluminum alloys and copper exhibit definite trends that are attributed to nonhydrodynamic or material strength effects. At moderate pressures (100 to 300 kb) the shock pressures and particle velocities corresponding to the higher speed impacts ( $V_I > 6$  km/sec) have a greater magnitude than is predicted by hydrodynamic theory such as the OIL code or the quasi-steady blast wave analysis. At low pressures ( $P_s < 100$  kb), the trend of the present data agrees with predictions that the pressure will decrease more rapidly in the stronger material. In the high pressure region of shock decay ( $P_s > 300$  kb), the data corresponding to  $V_I > 6$  km/sec agree reasonably well with the hydrodynamic OIL results and with GM/DRL's empirical formula, Eq. (14).

Agreement between the experimental data and OIL predictions seems to depend on impact velocity. This is demonstrated in Cases Al-3 and Al-4, which are moderate impact velocity conditions where  $V_I < C$ . The data from conditions Al-3 and Al-4 do not correlate with each other or with the hypervelocity impact data when hypervelocity scaling theory is applied (Fig. 15).

The present investigation has emphasized the need for additional experimentation and study of nonhydrodynamic or material strength effects on both moderate and hypervelocity impact phenomena.

### REFERENCES

1. Payne, J. J. "Summary of Impact Testing for NASA Project SUPER." AEDC-TR-66-97 (AD488517), September 1966.
2. Heyda, J. F. and Riney, T. D. "Peak Axial Pressures in Semi-Infinite Media under Hypervelocity Impact." Proceedings of the Seventh Hypervelocity Impact Symposium, Vol. III, Tampa, Florida, February 1965, pp. 75-122.
3. Heyda, J. F. and Riney, T. D. "Peak Pressures in Thick Targets Generated by Reduced Density Projectiles." NASA-CR-609, September 1966.
4. Gregson, V. C., Jr. "Optical Level Observation of Hypervelocity Impact Shock Waves." Journal of Applied Physics, Vol. 38, No. 4, March 15, 1967, pp. 1798-1802.

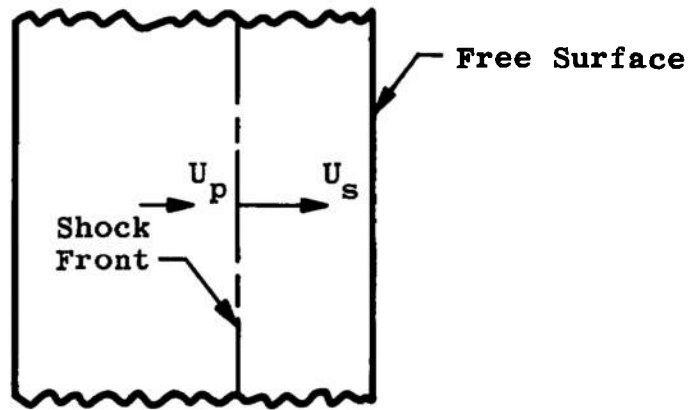
5. Walsh, John M. and Christian, Russell H. "Equation of State of Metals from Shock Wave Measurements." Physical Review, Vol. 97, No. 6, March 1955, pp. 1544-1556.
6. Walsh, J. M., Rice, M. H., McQueen, R. G., and Yarger, F. L. "Shock-Wave Compressions of Twenty-Seven Metals. Equations of State of Metals." Physical Review, Vol. 108, No. 2, October 1957, pp. 196-216.
7. McQueen, R. G. and Marsh, S. P. "Equation of State for Nineteen Metallic Elements from Shock-Wave Measurements to Two Megabars." Journal of Applied Physics, Vol. 31, No. 7, July 1960, pp. 1253-1269.
8. Charest, Jaques A. "Measurements of Shock Wave Pressures Generated by Hypervelocity Impacts in Aluminum." General Motors Corporation TR-64-58, November 1964. (Also in the Proceedings of the Seventh Hypervelocity Impact Symposium, Vol. V, pp. 161-211).
9. Johnson, W. E. "OIL - A Continuous Two-Dimensional Eulerian Hydrodynamic Code." GAMD-5580 (Revised) (AD477240), General Atomic Division of General Dynamics, January 7, 1965.
10. Dienes, J. K., Johnson, W. E., and Walsh, J. M. "Annual Status Report on the Theory of Hypervelocity Impact." GA-6509 (AD617540), General Atomic Division of General Dynamics, June 28, 1965.
11. Walsh, J. M. and Tillotson, J. H. "Hydrodynamics of Hypervelocity Impact." Proceedings of the Sixth Symposium on Hypervelocity Impact, Vol. II, Part I, August 1963, pp. 59-104, Cleveland, Ohio.
12. Walsh, J. M. and Johnson, W. E. "On the Theory of Hypervelocity Impact." Proceedings of the Seventh Symposium on Hypervelocity Impact, Vol. II, February 1965, pp. 1-75.
13. Taylor, G. I. "The Formation of a Blast Wave by a Very Intense Explosion; I. Theoretical Discussion; II. The Atomic Explosion of 1945." The Scientific Papers of G. I. Taylor, Vol. III, Aerodynamics and Mechanics of Projectiles and Explosions, University Press, Cambridge, England, September 1962, pp. 493-521. (Reprinted from Proceedings of the Royal Society, (A), Vol. CCI, 1950, pp. 159-186).
14. Sedov, L. I. Similarity and Dimensional Methods in Mechanics. Academic Press, New York, 1959.

15. Davids, N. and Huang, Y. K. "Shock Waves in Solid Craters." Journal of the Aero/Space Sciences, Vol. 29, No. 5, May 1962, pp. 550-552.
16. Davids, N., Calvit, H. H., and Johnson, O. T. "Spherical Shock Waves and Cavity Formation in Metals." Proceedings of the Sixth Symposium on Hypervelocity Impact, Vol. II, Part I, August 1963, pp. 229-271.
17. Rae, William J. and Kirchner, Henry P. "A Blast-Wave Theory of Crater Formation in Semi-Infinite Targets." Proceedings of the Sixth Symposium on Hypervelocity Impact, Vol. II, Part I, August 1963, pp. 163-227.
18. Ōshima, J. "Blast Waves Produced by Exploding Wire." Aero Research Institute, University of Tokyo, Report No. 358, July 1960. (Also Exploding Wires, Vol. 2, Edited by W. G. Chase and H. K. Moore, Plenum Press, New York, 1962, pp. 159-174.
19. Rae, William J. "Nonsimilar Solutions for Impact-Generated Shock Propagation in Solids." NASA CR-54251, CAL AI-1821-A-2, March 1965.
20. Heyda, J. F. "Shock Front Variation in Time for High Speed Impact into Water." Proceedings of the Sixth Symposium on Hypervelocity Impact, Vol. II, Part I, August 1963, pp. 321-336.
21. Riney, T. D. "Theory of High Speed Impact." (Summary Report, November 3, 1960-November 2, 1961) APGC TDR-62-20 (AD274048), General Electric Space Sciences Laboratory, March 1962.
22. Riney, T. D. "PIC Formulation of Visco-Plastic Model for Hypervelocity Impact." APGC TDR 62-24, General Electric Space Sciences Laboratory, July 1962.
23. Piacesi, Robert and Watt, James A. "A Study of the Role of Mechanical-Strength Properties on the Phenomenon of Spallation." NOL TR-66-42, January 4, 1966.
24. Bach, G. and Lee, J. H. "Shock Propagation in Solid Media." AIAA Paper No. 67-141, presented at the 5th AIAA Aerospace Sciences Meeting, New York, January 23-26, 1967.
25. Whitesides, J. L. "A Theoretical Solution of the Hypervelocity Impact Problem." Ph.D. Dissertation, University of Texas, August 1968.

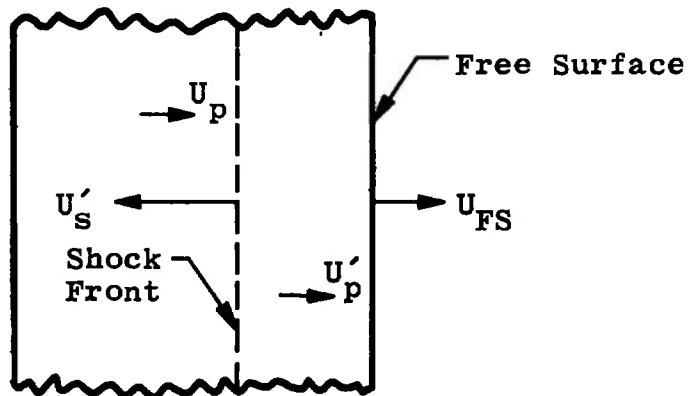
26. Mok, Chi-Hung. "The Effects of Solid Strength on the Propagation and Attenuation of Spherical and Plane Shock Waves." BRL Report No. 1375, October 1967.
27. Frasier, J. T., Karpov, B. G., and Holloway, L. S. "The Behavior of Wax Targets Subjected to Hypervelocity Impacts." Proceedings of the Seventh Hypervelocity Impact Symposium, Vol. V, Experiments, February 1965, pp. 123-160.
28. Riney, T. D. and Heyda, J. F. "Hypervelocity Impact Calculations." Proceedings of the Seventh Hypervelocity Impact Symposium, Vol. II, Theory, February 1965, pp. 77-185.
29. Rae, William J. "A Critical Review of Impact Theories." Paper presented at the Highwater Conference on Meteoroid Impact, Highwater, Quebec, July 14-15, 1966.
30. Titterton, George F. Aircraft Materials and Processes. Pittman Publishing Corporation, New York, 1956.
31. Payne, J. J. and Johnson, R. E. Data from mechanical tests performed in the AEDC Engineering Support Facility, Metallurgical Laboratory.

**APPENDIXES**

- I. ILLUSTRATIONS**
- II. HYDRODYNAMIC OIL CODE PREDICTIONS**
- III. TABULATION OF EXPERIMENTAL DATA**
- IV. NAVAL ORDNANCE LABORATORY EXPERIMENTAL DATA**
- V. TARGET MATERIAL YIELD STRENGTH**

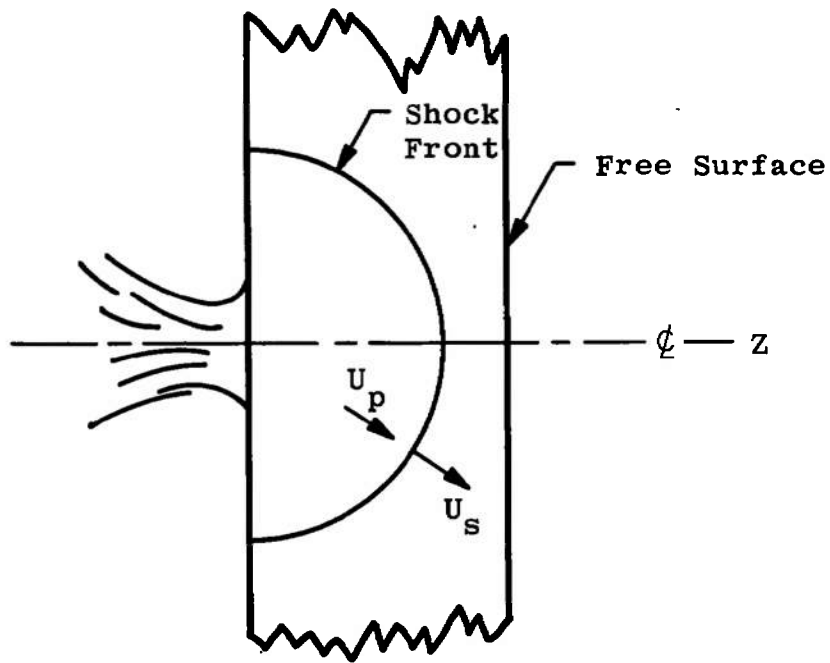


a. Before Reflection

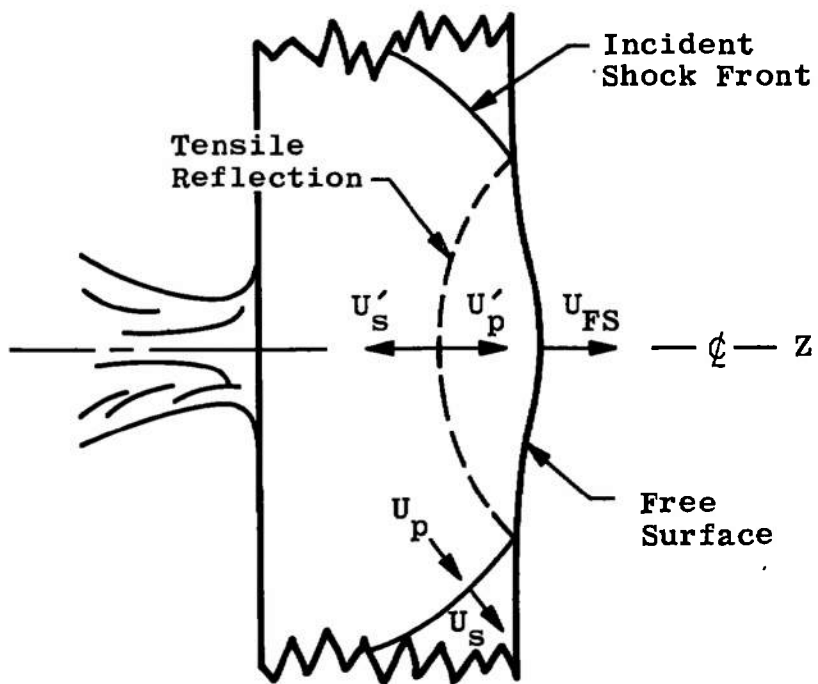


b. After Reflection

Fig. 1 Plane Shock Geometry

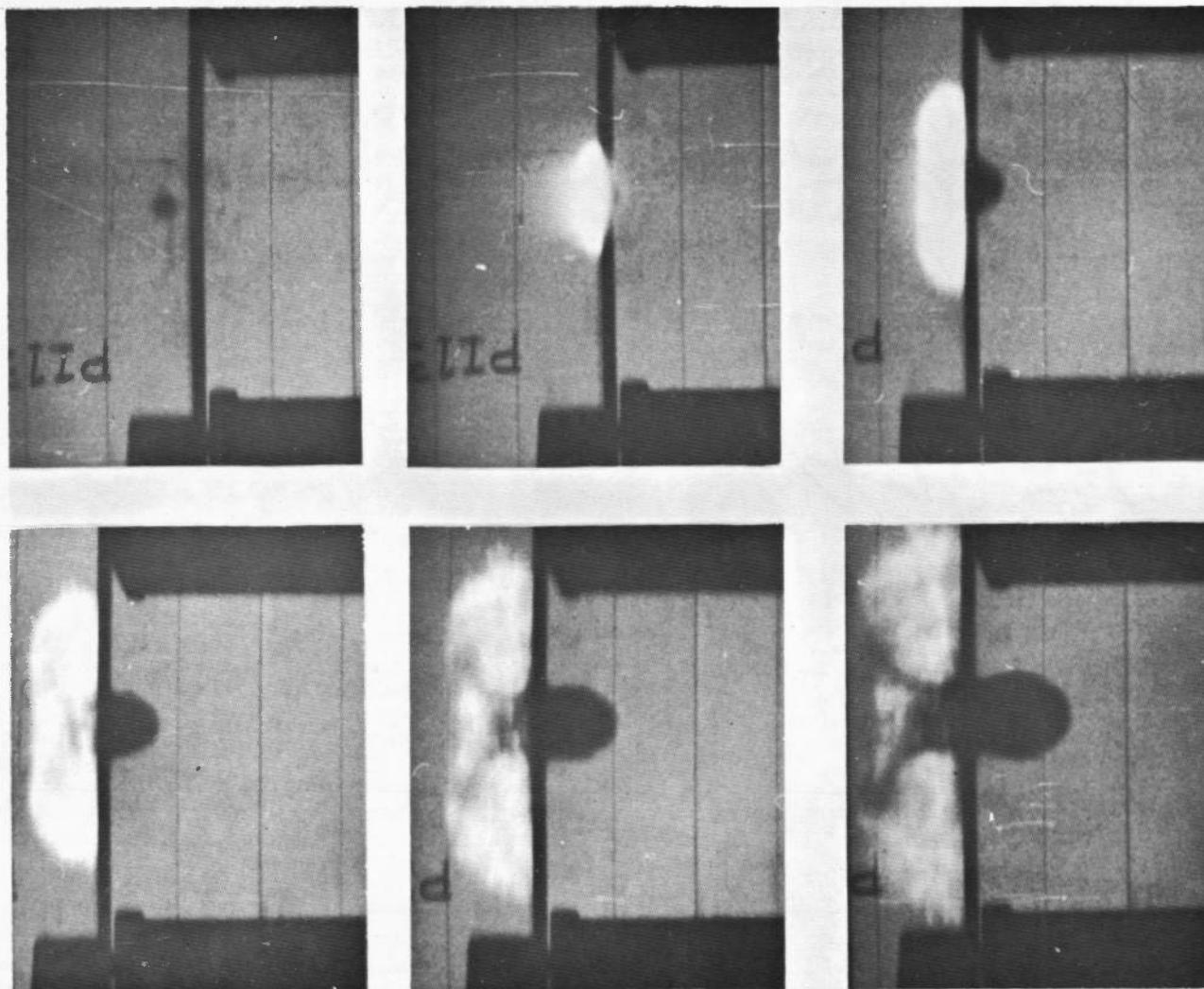


a. Before Reflection



b. After Reflection

Fig. 2 Simplified Hemispherical Shock Geometry



$$V_I = 7.48 \text{ km/sec}, d_p = 0.635 \text{ cm}, T = 0.317 \text{ cm}$$

Fig. 3 Beckman & Whitley High-Speed Framing Camera Sequential Photographs for Shot PI-13

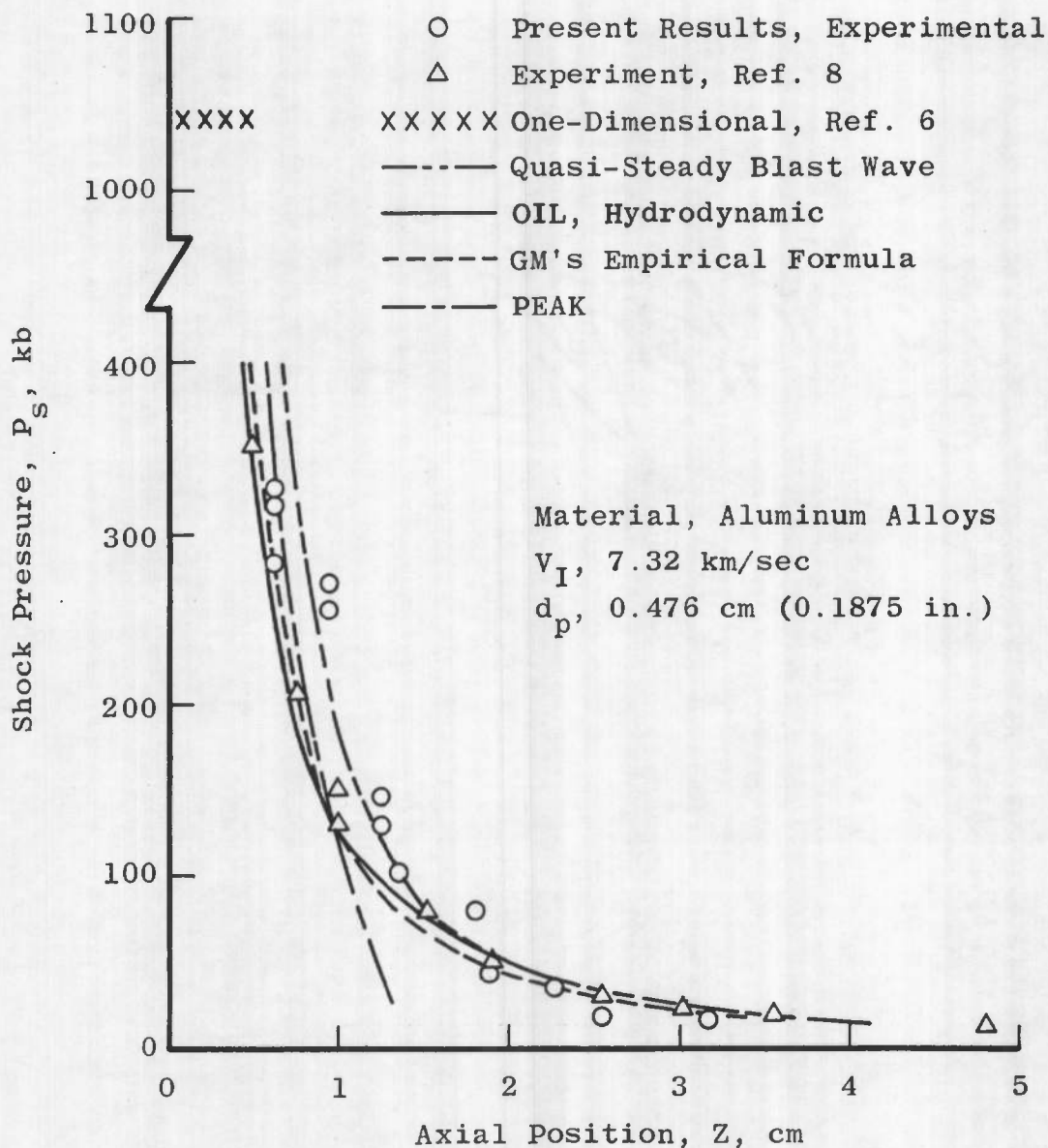


Fig. 4 Comparison of Experimental and Theoretical Pressure Data for Case Al-1

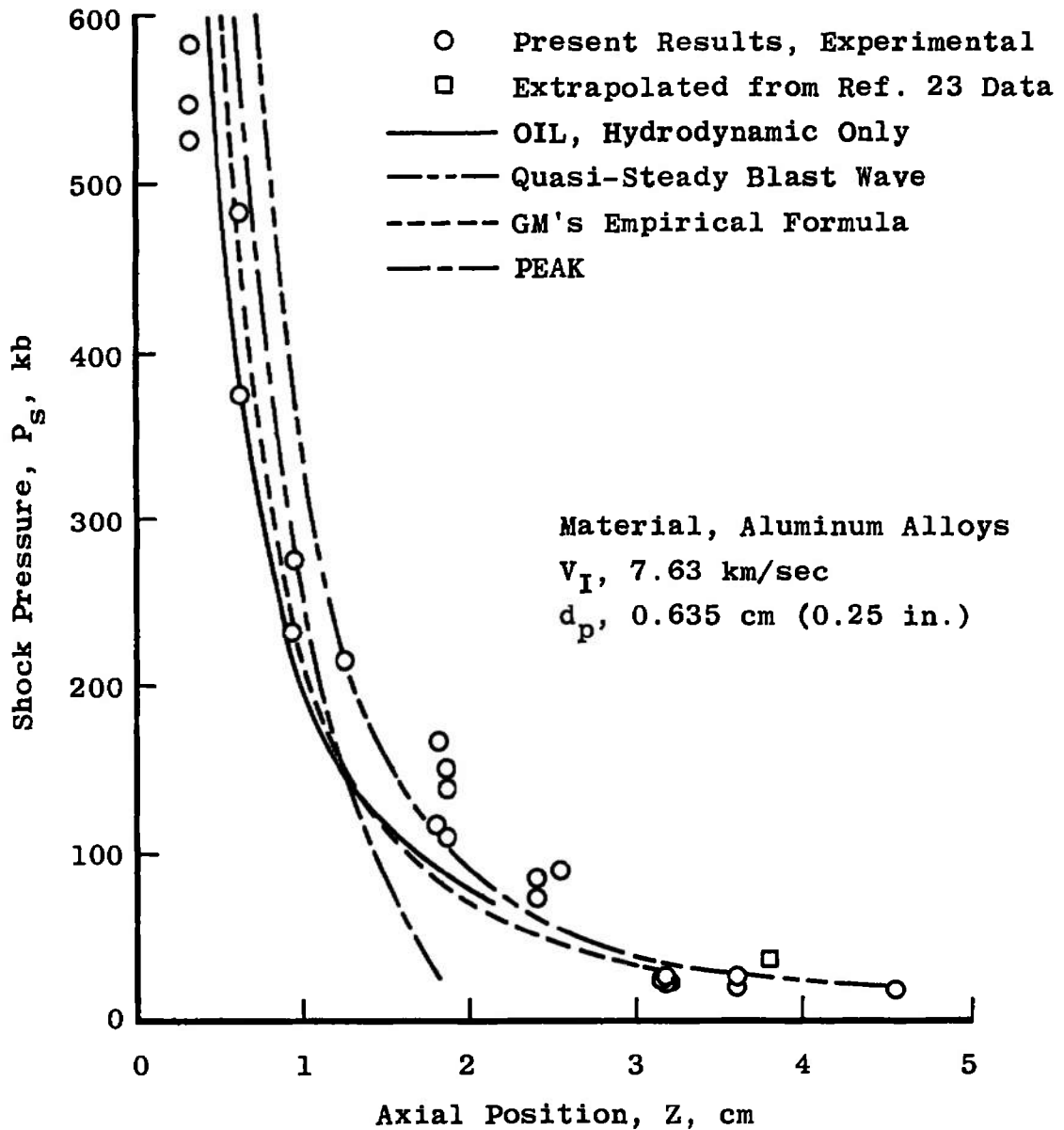


Fig. 5 Comparison of Experimental and Theoretical Pressure Data for Case A1-2

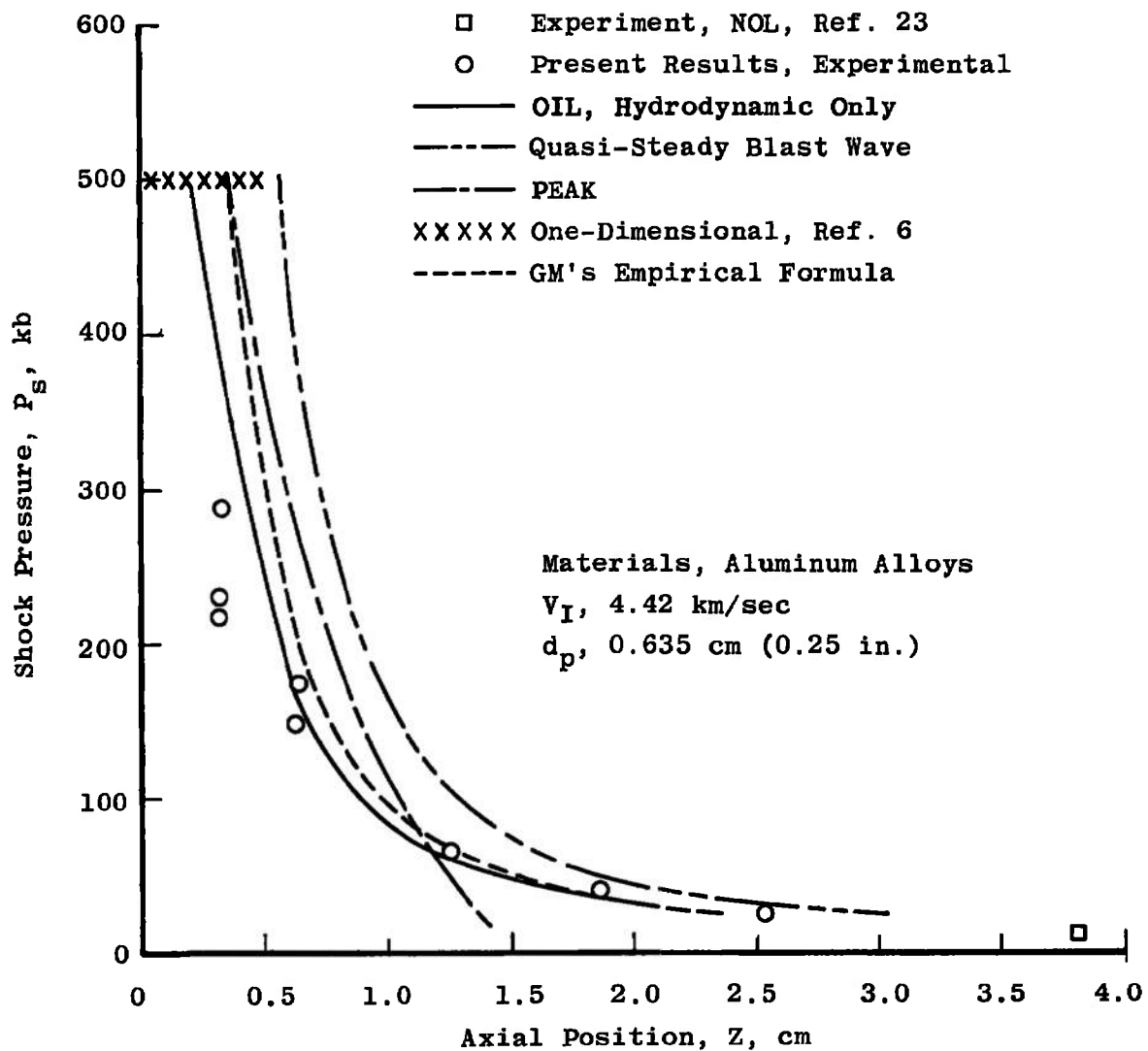


Fig. 6 Comparison of Experimental and Theoretical Pressure Data for Case A1-3

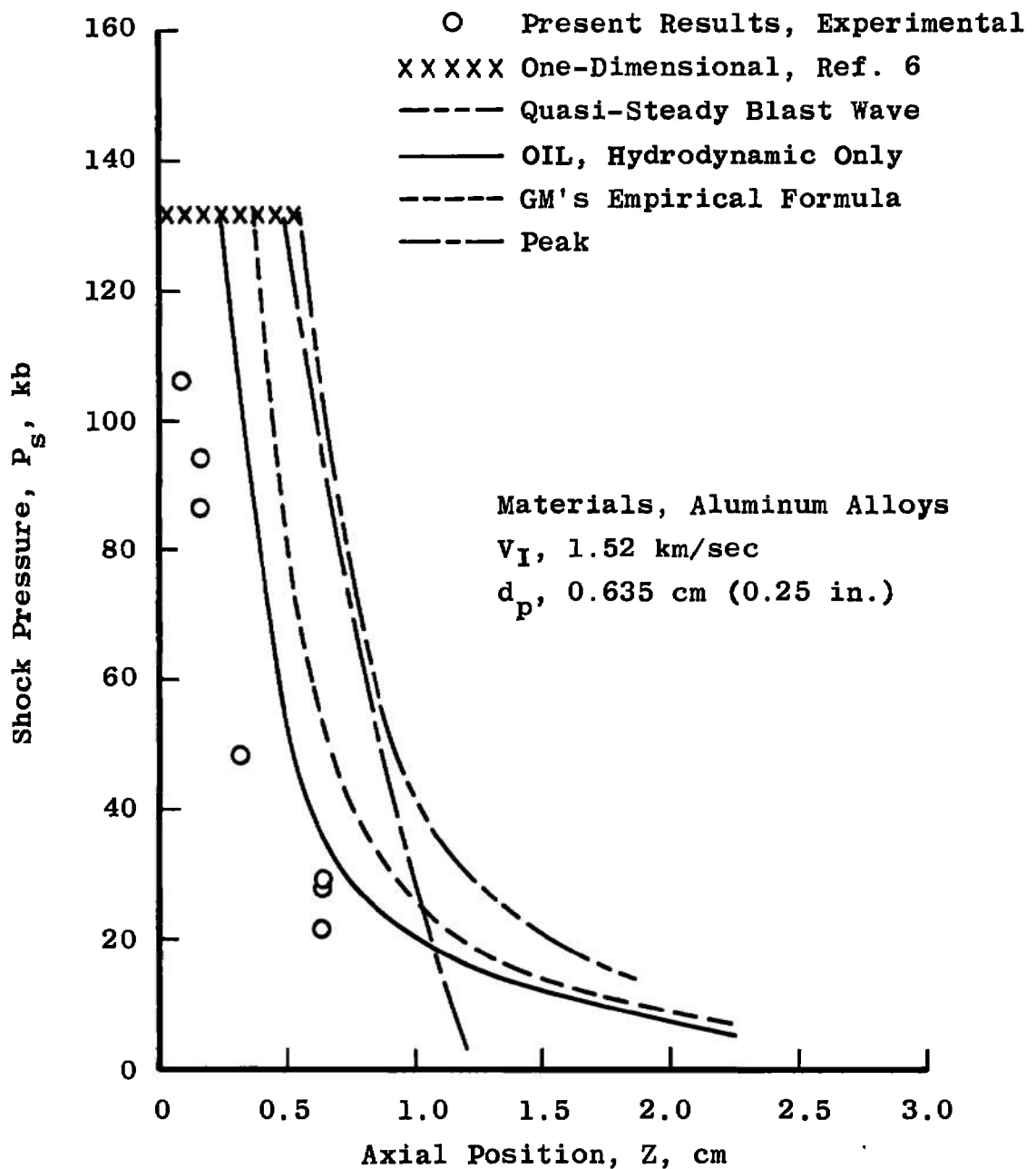


Fig. 7 Comparison of Experimental and Theoretical Pressure Data for Case Al-4

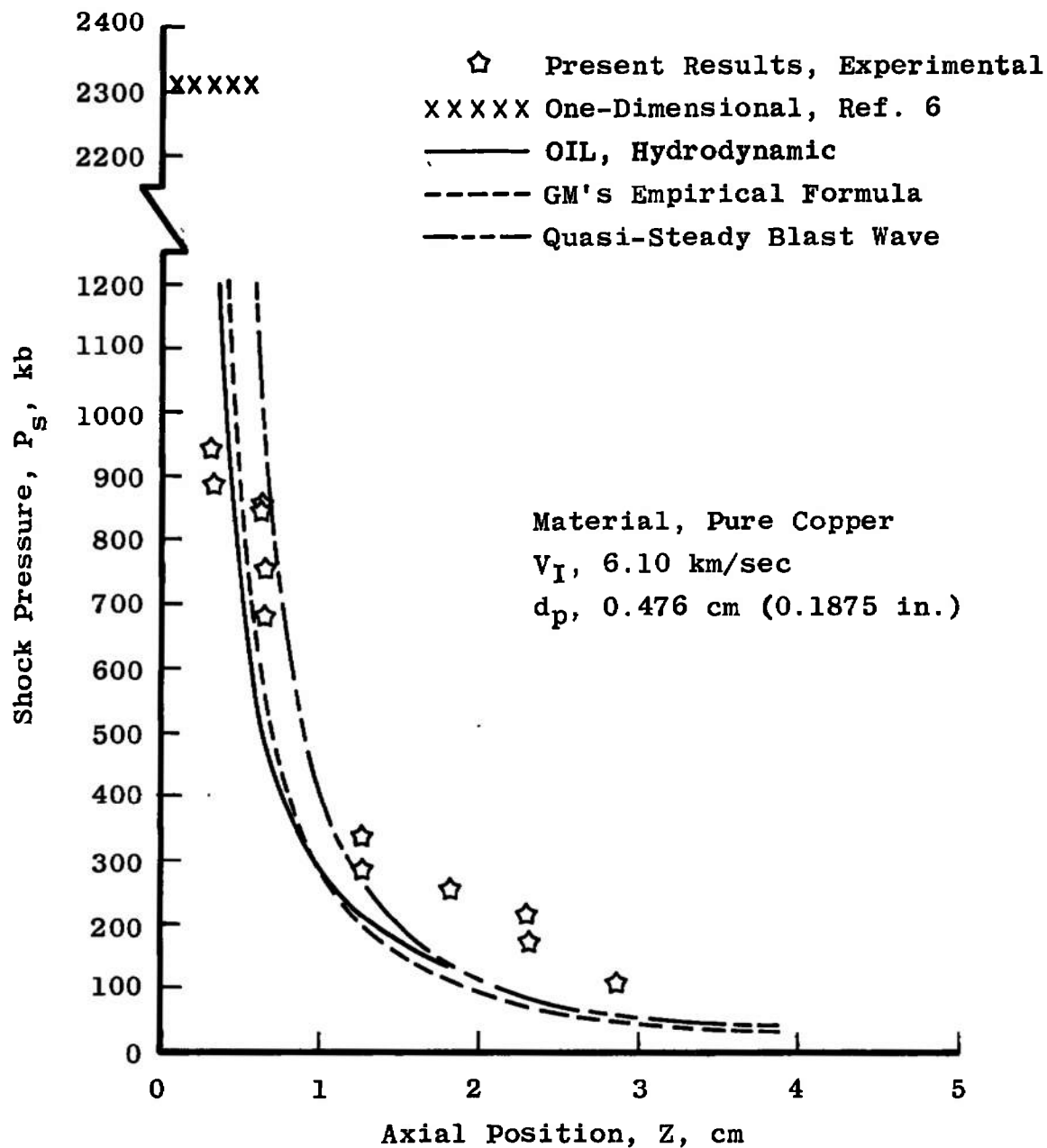


Fig. 8 Comparison of Experimental and Theoretical Pressure Data for Case Cu-1

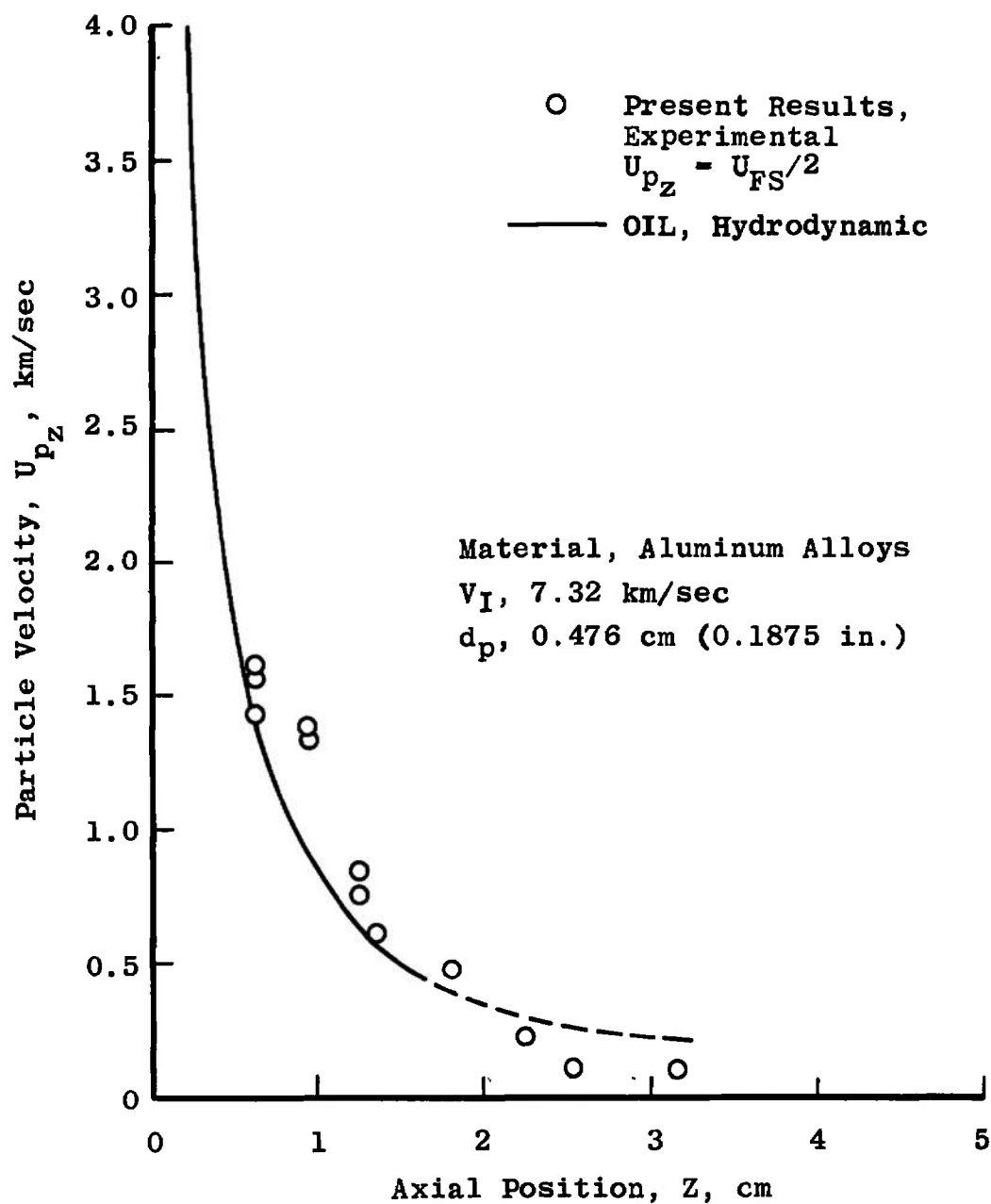


Fig. 9 Comparison of Experimental and Theoretical Particle Velocity for Case Al-1

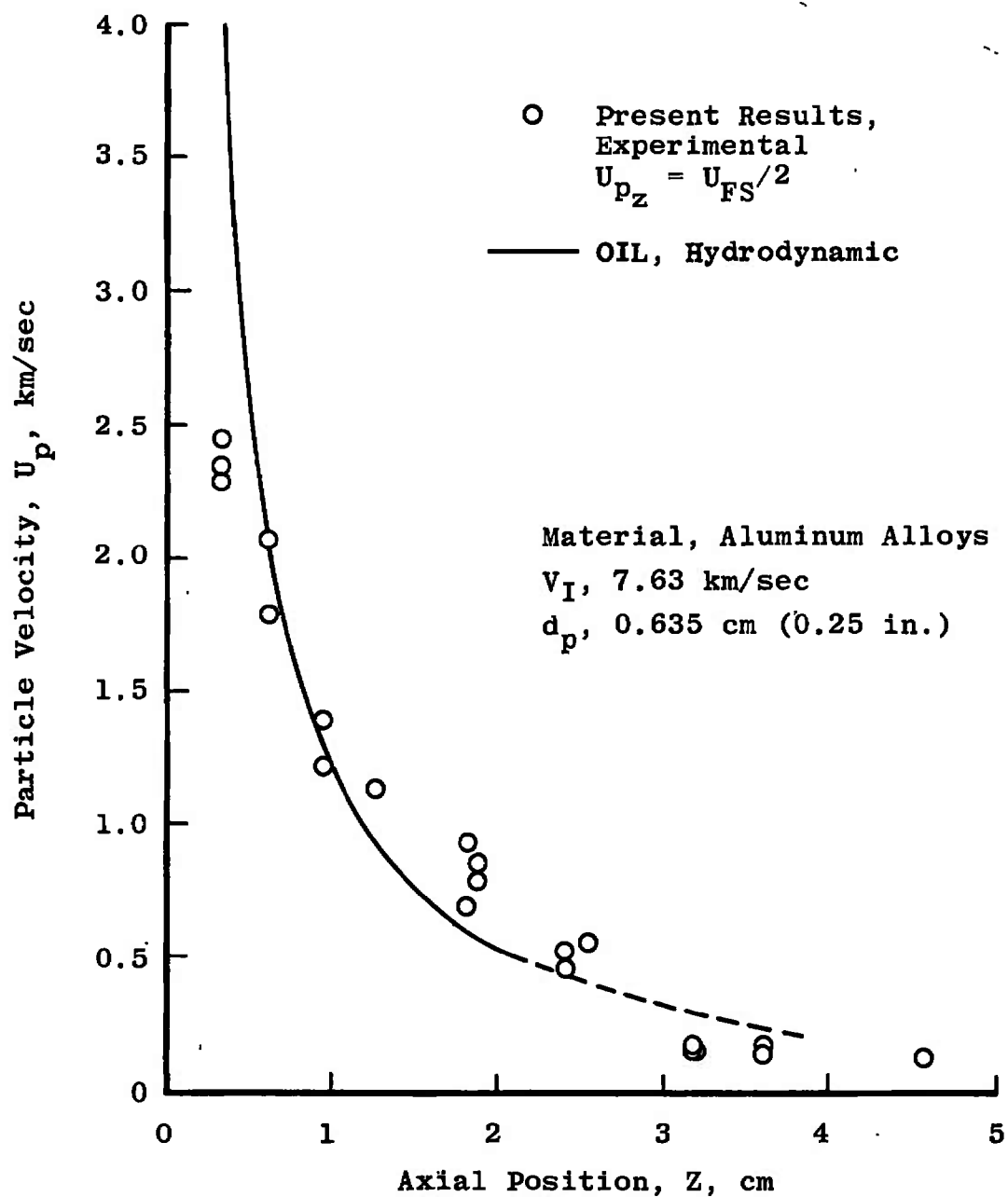


Fig. 10 Comparison of Experimental and Theoretical Particle Velocity for Case Al-2

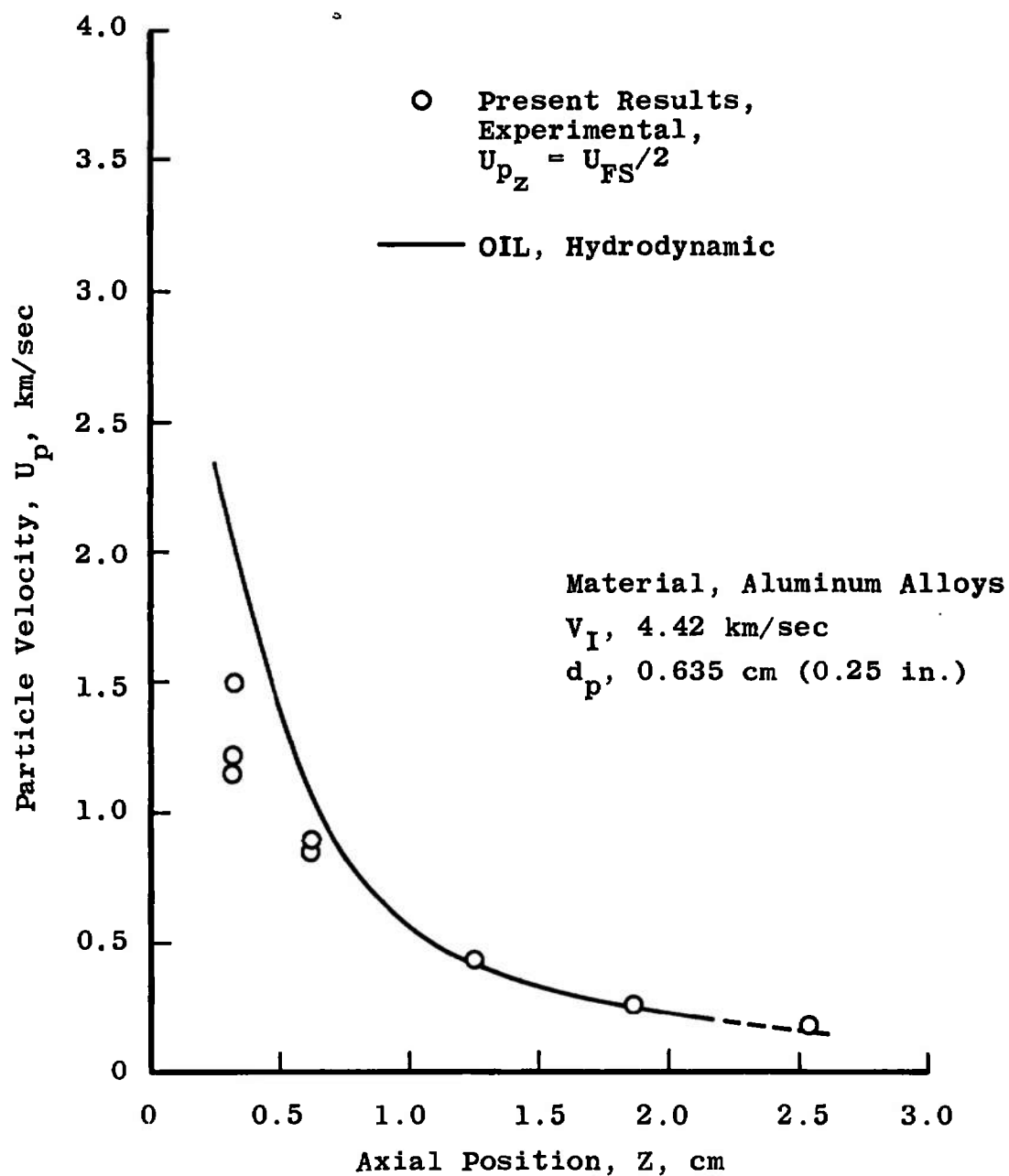


Fig. 11 Comparison of Experimental and Theoretical Particle Velocity for Case Al-3

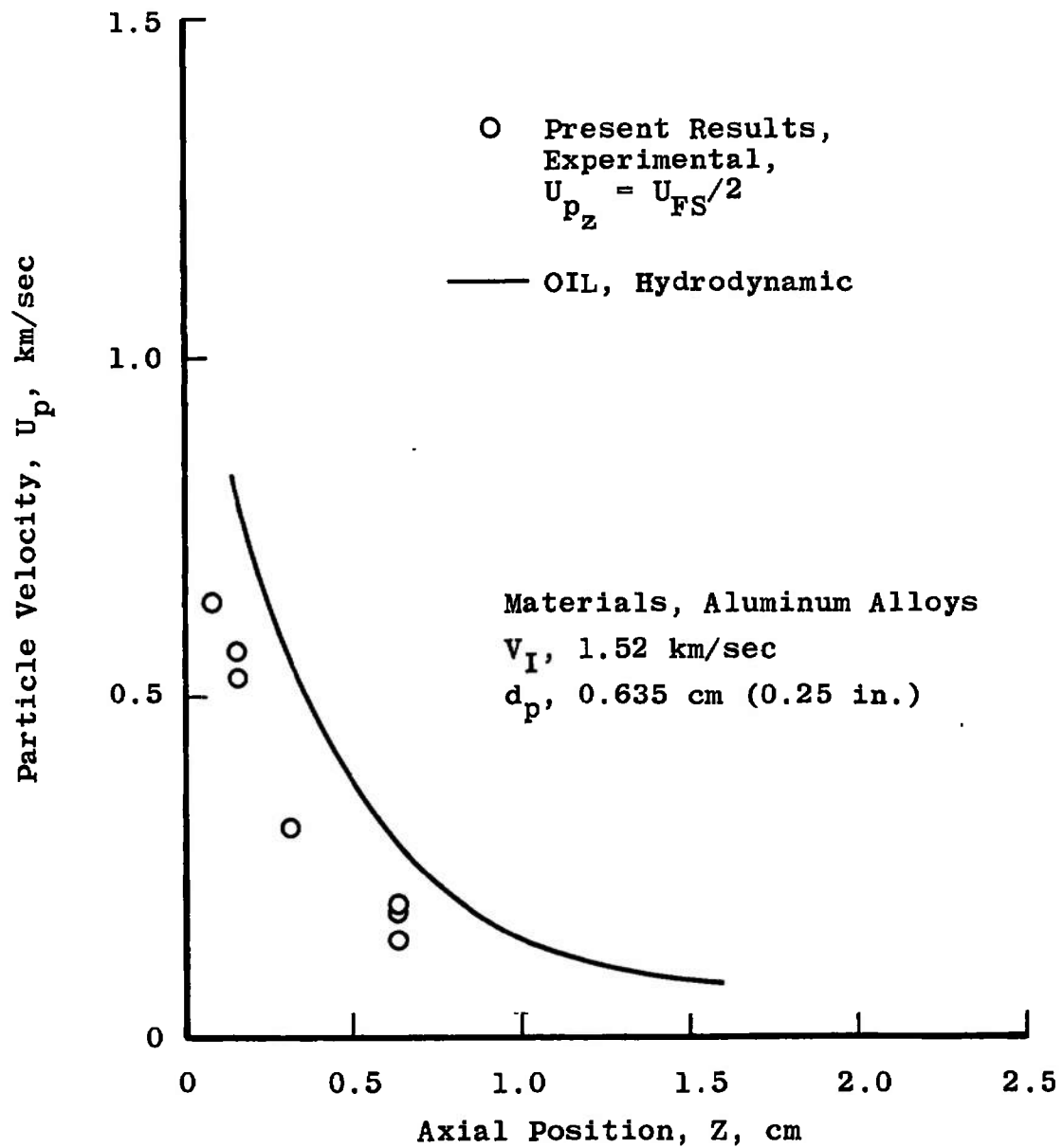


Fig. 12 Comparison of Experimental and Theoretical Particle Velocity for Case Al-4

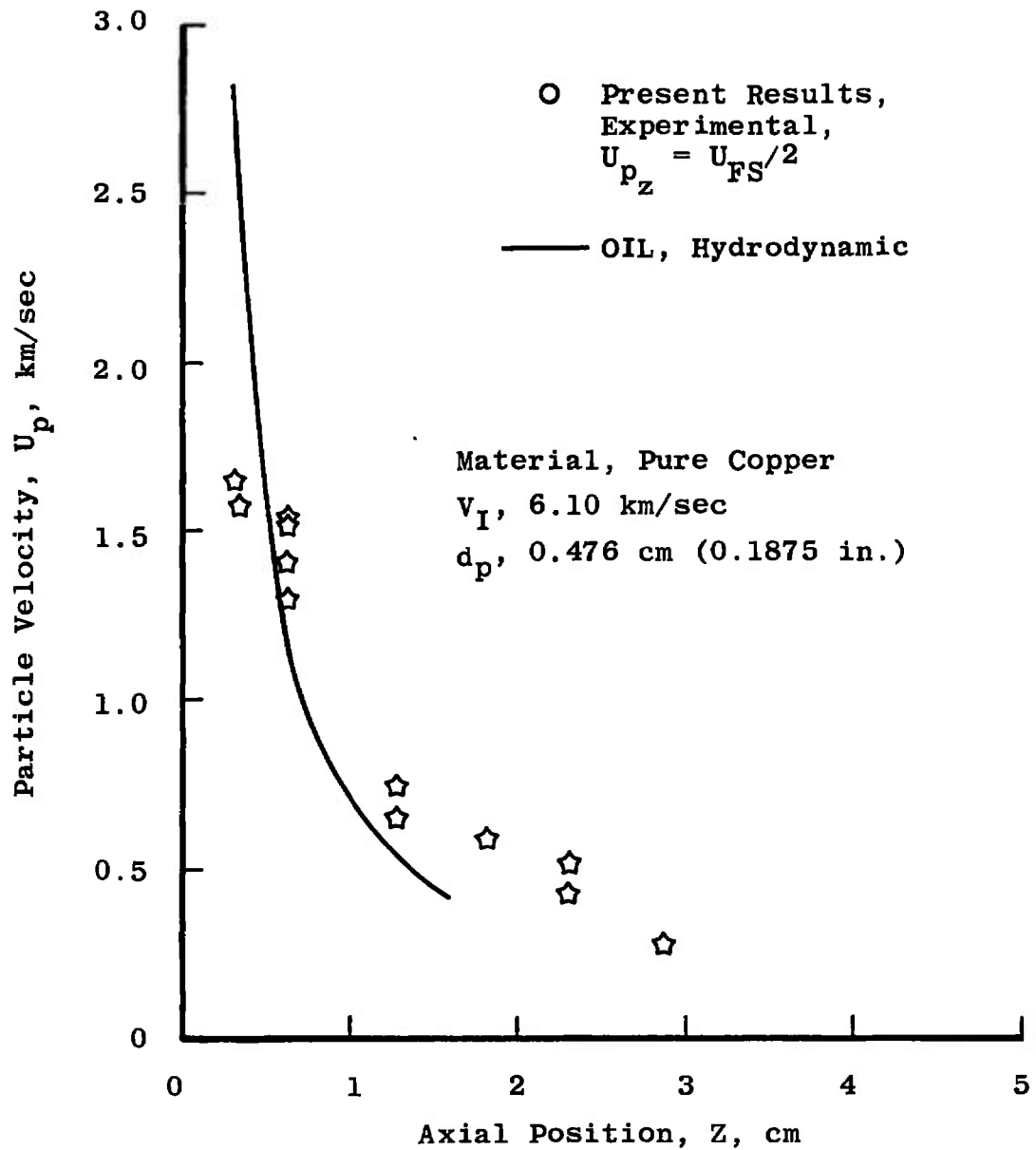


Fig. 13 Comparison of Experimental and Theoretical Particle Velocity for Case Cu-1

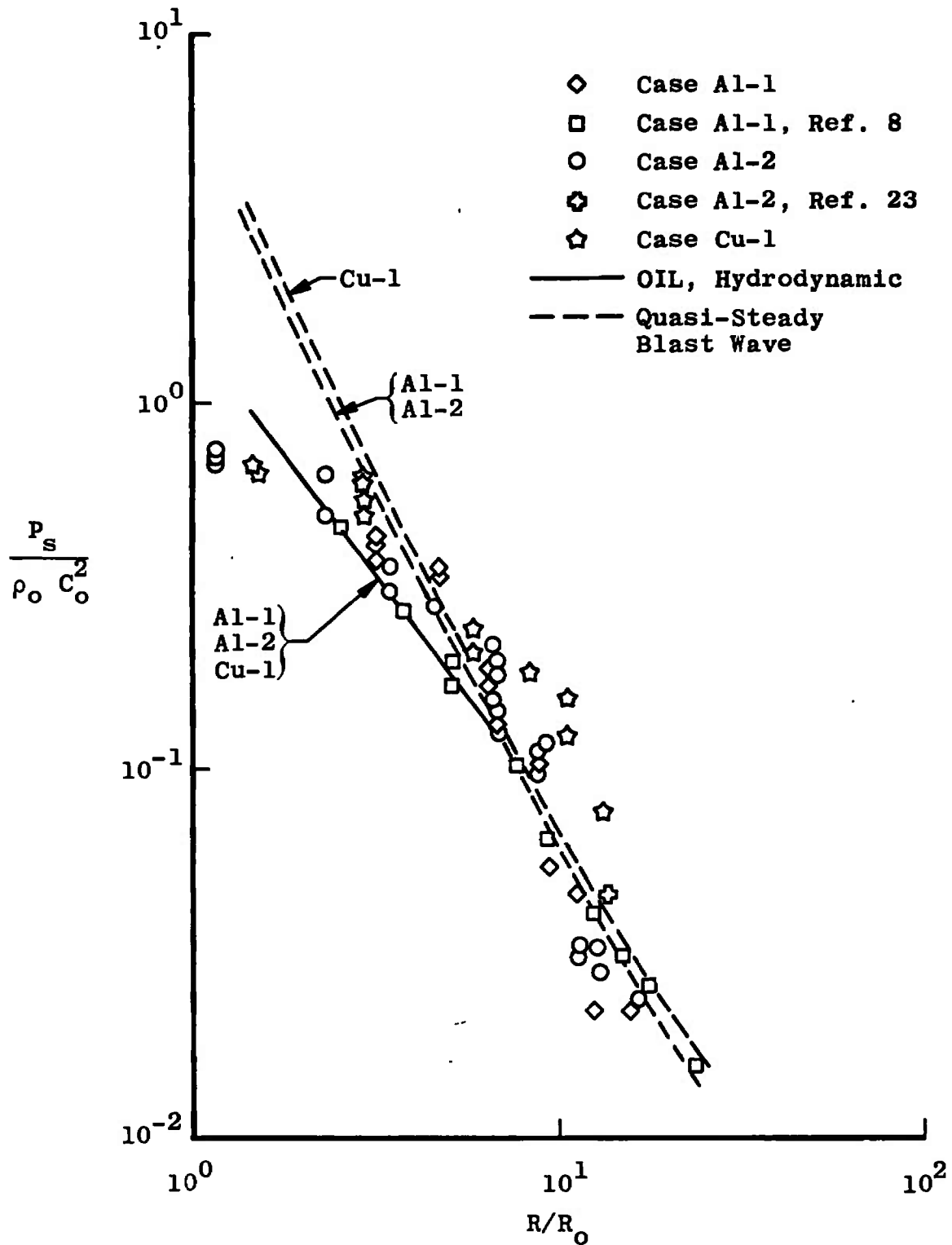


Fig. 14 Normalized Results for Conditions A1-1, A1-2, and Cu-3

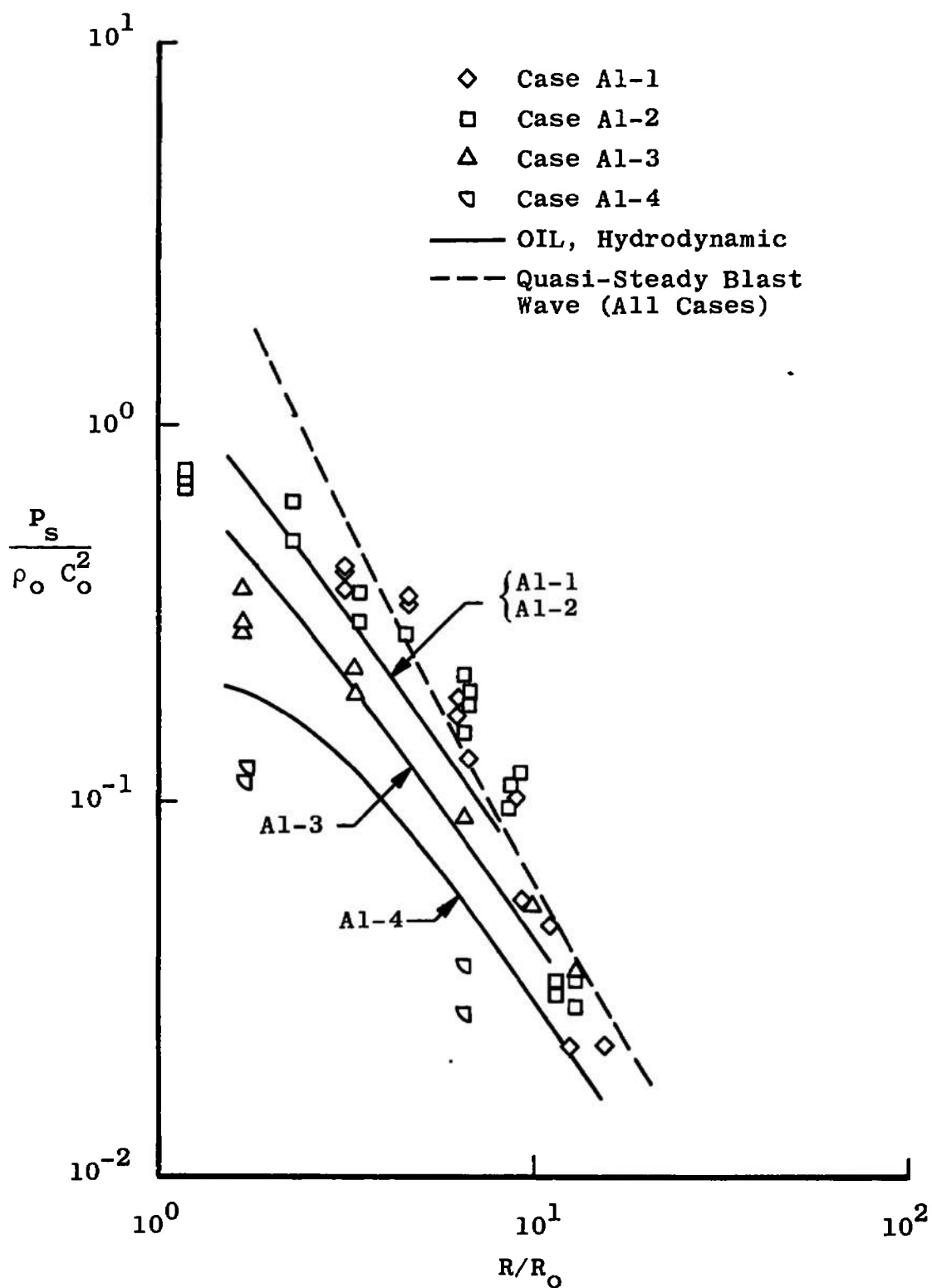


Fig. 15 Normalized Results for Conditions A1-1, A1-2, A1-3, and A1-4

## APPENDIX II

### HYDRODYNAMIC OIL CODE PREDICTIONS

A tabulation of the results from the hydrodynamic OIL code (Refs. 9 and 10) for high velocity impact is contained in this appendix. The following table lists the pertinent dimensions of the target and projectiles used in the computations. The cross-section grid of the target and projectile is shown in Fig. II-1.

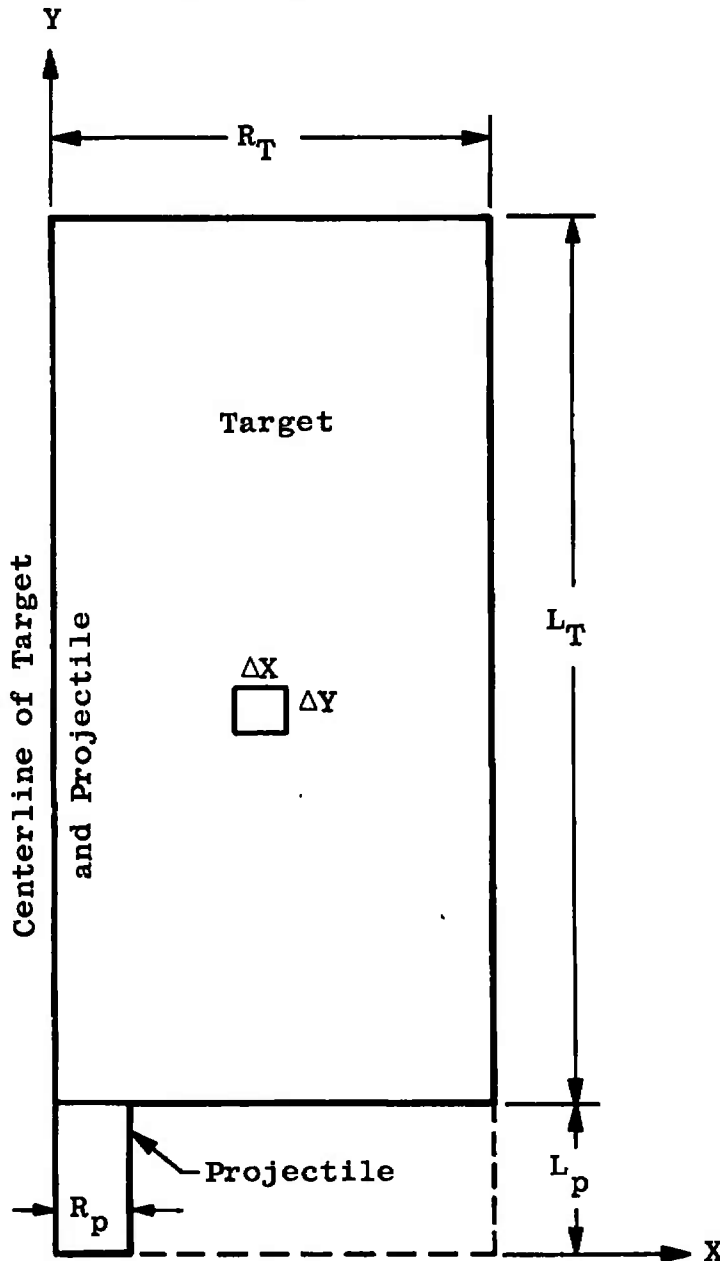


Fig. II-1 Radial Cross Section of Target and Projectile  
for OIL Computer Code

**TABLE II-1**  
**TARGET AND PROJECTILE DIMENSIONS**

Case No.	$V_I$ , km/sec	$R_p$ , cm	$L_p$ , cm	$R_T$ , cm	$L_T$ , cm	$\Delta X$ , cm	$\Delta Y$ , cm
Al-1	7.32	0.2076	0.4152	1.107	1.800	0.0346	0.0346
Al-2	7.63	0.2760	0.5520	1.329	2.242	0.0460	0.0460
Al-3	4.42	0.2760	0.5520	1.329	2.242	0.0460	0.0460
Al-4	1.52	0.2760	0.5520	1.329	2.242	0.0460	0.0460
Cu-1	6.10	0.2076	0.4152	1.107	1.800	0.0346	0.0346

The values of  $P_s$  in the following tables were the maximum values nearest the target axis of symmetry for a given computation cycle.

**TABLE II-2**  
**HYDRODYNAMIC OIL CODE PREDICTION FOR CASE AI-1**

Cycle	Z, cm	Time, $\mu$ sec	$P_s$ , kb	$\frac{\rho_s}{\rho_o}$	$U_p$ , km/sec	$\frac{Z}{R_o}$	$\frac{P_s}{\rho_o C_o^2}$
20	0.035	0.105	1296	1.576	3.619	0.170	1.677
40	0.173	0.210	1102	1.573	3.940	0.850	1.426
60	0.277	0.315	774	1.469	3.330	1.360	1.001
80	0.381	0.420	506	1.245	2.435	1.870	0.655
100	0.450	0.525	391	1.308	2.103	2.210	0.506
120	0.519	0.630	307	1.262	1.770	2.550	0.397
140	0.588	0.735	255	1.229	1.518	2.890	0.330
160	0.657	0.840	220	1.206	1.332	3.231	0.285
180	0.727	0.945	194	1.187	1.189	3.570	0.251
200	0.800	1.050	174	1.172	1.071	3.910	0.225
240	0.934	1.261	142	1.146	0.881	4.591	0.184
280	1.038	1.471	116	1.124	0.766	5.101	0.150
320	1.176	1.681	104	1.103	0.673	5.781	0.135
360	1.315	1.891	89	1.099	0.573	6.461	0.115
400	1.419	2.101	82	1.092	0.539	6.971	0.106
440	1.522	2.311	72	1.082	0.487	7.481	0.093
480	1.661	2.521	67	1.077	0.443	8.161	0.087

**TABLE II-3**  
**HYDRODYNAMIC OIL CODE PREDICTION FOR CASE AI-2**

Cycle	Z, cm	Time, $\mu$ sec	P <sub>s</sub> , kb	$\frac{\rho_s}{\rho_o}$	U <sub>p</sub> , km/sec	$\frac{Z}{R_o}$	$\frac{P_s}{\rho_o C_o^2}$
20	0.046	0.134	1377	1.595	3.829	0.165	1.781
40	0.230	0.268	1158	1.589	4.041	0.826	1.498
60	0.368	0.402	826	1.487	3.417	1.322	1.069
80	0.460	0.536	557	1.381	2.904	1.653	0.721
100	0.598	0.670	423	1.323	2.171	2.149	0.547
120	0.690	0.804	341	1.281	1.860	2.479	0.441
140	0.782	0.938	284	1.248	1.607	2.810	0.367
160	0.874	1.072	245	1.222	1.409	3.141	0.317
180	0.966	1.206	214	1.201	1.248	3.471	0.277
200	1.058	1.340	188	1.182	1.109	3.802	0.243
220	1.104	1.474	167	1.166	1.058	3.967	0.216
240	1.196	1.608	156	1.157	0.979	4.298	0.202
260	1.288	1.742	145	1.148	0.903	4.628	0.188
280	1.380	1.876	133	1.138	0.827	4.959	0.172
300	1.472	2.010	120	1.127	0.748	5.289	0.155
320	1.518	2.144	114	1.122	0.739	5.455	0.148
340	1.610	2.278	108	1.117	0.694	5.785	0.140
360	1.702	2.412	100	1.109	0.640	6.116	0.129
380	1.794	2.546	91	1.101	0.580	6.446	0.118
400	1.840	2.679	91	1.101	0.593	6.612	0.118
440	1.978	2.947	80	1.091	0.538	7.107	0.104
480	2.162	3.215	74	1.084	0.484	7.769	0.095

TABLE II-4  
HYDRODYNAMIC OIL CODE PREDICTION FOR CASE AI-3

Cycle	Z, cm	Time, $\mu$ sec	P <sub>s</sub> , kb	$\frac{\rho_s}{\rho_o}$	U <sub>p</sub> , km/sec	$\frac{Z}{R_o}$	$\frac{P_s}{\rho_o C_o^2}$
20	0.046	0.193	613	1.374	2.046	0.238	0.793
30	0.138	0.290	557	1.364	2.373	0.713	0.721
40	0.230	0.387	480	1.345	2.339	1.188	0.621
50	0.322	0.483	400	1.311	2.096	1.663	0.518
60	0.414	0.580	320	1.268	1.729	2.138	0.414
70	0.460	0.677	240	1.2185	1.545	2.376	0.311
80	0.552	0.773	206	1.195	1.258	2.851	0.267
90	0.598	0.870	173	1.172	1.130	3.089	0.224
100	0.690	0.967	143	1.147	0.890	3.564	0.185
110	0.736	1.063	130	1.137	0.851	3.802	0.168
120	0.782	1.160	118	1.126	0.789	4.039	0.153
130	0.828	1.257	105	1.114	0.728	4.277	0.136
140	0.874	1.353	93	1.104	0.663	4.515	0.120
150	0.966	1.450	87	1.098	0.585	4.990	0.113
160	1.012	1.547	82	1.092	0.561	5.227	0.106
170	1.058	1.643	77	1.087	0.530	5.465	0.100
180	1.104	1.740	71	1.081	0.500	5.703	0.092
190	1.150	1.837	65	1.079	0.467	5.940	0.084
200	1.242	1.933	61	1.071	0.418	6.415	0.079
220	1.334	2.127	56	1.066	0.390	6.891	0.072
240	1.426	2.320	50	1.060	0.357	7.366	0.065
260	1.564	2.513	44	1.053	0.308	8.079	0.057
280	1.656	2.707	41.5	1.050	0.292	8.554	0.054
300	1.747	2.900	38.5	1.047	0.274	9.024	0.050
320	1.840	3.093	35.3	1.043	0.255	9.504	0.046
340	1.978	3.286	32.5	1.040	0.228	10.217	0.042
360	2.110	3.480	30.8	1.038	0.219	10.899	0.040
380	2.162	3.673	29.1	1.036	0.207	11.167	0.038

TABLE II-5  
HYDRODYNAMIC OIL CODE PREDICTION FOR CASE AI-4

Cycle	Z, cm	Time, $\mu$ sec	P <sub>s</sub> , kb	$\frac{\rho_s}{\rho_o}$	U <sub>p</sub> , km/sec	$\frac{Z}{R_o}$	$\frac{P_s}{\rho_o C_o^2}$
20	0.046	0.193	210	1.191	0.765	0.483	0.272
40	0.138	0.387	161	1.159	0.820	1.450	0.208
60	0.322	0.580	106	1.115	0.542	3.382	0.137
80	0.414	0.773	82	1.092	0.495	4.349	0.106
100	0.506	0.967	55	1.065	0.384	5.315	0.071
120	0.597	1.160	37	1.046	0.289	6.282	0.048
140	0.750	1.353	29	1.036	0.254	7.878	0.037
160	0.874	1.547	25	1.031	0.165	9.181	0.032
180	0.966	1.739	22	1.028	0.148	10.147	0.029
200	1.058	1.933	20	1.025	0.133	11.113	0.025
240	1.242	2.320	16	1.020	0.108	13.046	0.020
280	1.426	2.707	12	1.016	0.089	14.979	0.016
320	1.610	3.093	10	1.013	0.073	16.912	0.013
360	1.886	3.480	9	1.011	0.058	19.811	0.011
400	2.116	3.866	6	1.008	0.050	22.227	0.008

**TABLE II-6**  
**HYDRODYNAMIC OIL CODE PREDICTION FOR CASE C<sub>0</sub>-1**

Cycle	Z, cm	Time, μsec	P <sub>s</sub> , kb	$\frac{\rho_s}{\rho_o}$	U <sub>p</sub> , km/sec	$\frac{Z_i}{R_o}$	$\frac{P_s}{\rho_o C_o^2}$
20	0.035	0.126	3065	1.553	3.694	0.157	2.199
30	0.104	0.189	2818	1.570	3.474	0.472	2.022
40	0.173	0.252	2529	1.592	3.339	0.786	1.814
50	0.208	0.315	2024	1.523	3.202	0.944	1.452
60	0.277	0.378	1716	1.496	2.826	1.258	1.232
70	0.311	0.441	1413	1.447	2.568	1.416	1.014
80	0.346	0.505	1129	1.395	2.309	1.573	0.810
90	0.415	0.568	944	1.359	2.060	1.887	0.677
100	0.450	0.631	845	1.338	1.848	2.045	0.606
110	0.484	0.694	756	1.317	1.673	2.202	0.542
120	0.519	0.757	681	1.297	1.532	2.359	0.489
130	0.554	0.820	617	1.278	1.417	2.516	0.442
140	0.588	0.883	564	1.262	1.324	2.674	0.404
150	0.623	0.946	517	1.246	1.246	2.831	0.371
160	0.623	1.009	482	1.236	1.179	2.831	0.346
170	0.657	1.012	460	1.228	1.119	2.988	0.330
180	0.692	1.135	440	1.221	1.065	3.145	0.316
190	0.727	1.198	421	1.213	1.014	3.303	0.302
200	0.865	1.438	344	1.184	0.860	3.932	0.247
210	0.969	1.723	287	1.158	0.739	4.404	0.206
220	1.107	2.008	253	1.143	0.643	5.033	0.182
230	1.246	2.292	220	1.128	0.555	5.662	0.158
240	1.349	2.577	192	1.114	0.511	6.134	0.138
250	1.488	2.861	176	1.106	0.458	6.763	0.126

### APPENDIX III

#### TABULATION OF EXPERIMENTAL DATA

A tabulation of the present data is given in this appendix. A portion of the present data was obtained by reexamination of B&W film records from AEDC test shots for NASA Project SUPER (Support Program for Extra-Terrestrial Research). Reference 1 is a summary of AEDC impact test results for NASA Project SUPER. The data for Case A1-4 were obtained with a smooth bore powder gun instead of the usual two-stage light-gas gun.

TABLE III-1  
DATA TABULATION FOR CASE AI-1

Shot No.	V <sub>I</sub> , ft/sec	V <sub>I</sub> , km/sec	Target Thickness, in.	Target Thickness, cm	UFS Measured, ft/sec	UFS, km/sec	P <sub>s</sub> , kb	$\frac{R}{R_0}$	$\frac{P_s}{\rho_0 C_0^2}$
124	24,600	7.498	0.249	0.632	9408	2.868	283	3.109	0.366
156	25,040	7.632	0.249	0.632	10,561	3.219	328	3.109	0.424
158	25,511	7.776	0.249	0.632	10,250	3.124	316	3.109	0.409
160	24,927	7.598	0.373	0.948	8691	2.649	256	4.657	0.331
163	24,446	7.451	0.498	1.265	4933	1.504	129	6.217	0.167
165	23,306	7.103	0.498	1.265	5484	1.672	146	6.217	0.189
166	22,311	6.800	0.747	1.897	1783	0.543	42	9.326	0.054
185	24,110	7.349	1.251	3.178	738	0.225	17	15.618	0.022
189	23,548	7.178	0.373	0.948	9088	2.770	271	4.657	0.351
315*	25,400	7.742	0.535	1.360	3722	1.209	101	6.679	0.131
316*	24,700	7.529	0.713	1.810	3184	0.971	79	8.901	0.102
317*	26,100	7.955	0.890	2.260	1516	0.462	35	11.111	0.046
318*	25,700	7.833	1.000	2.54	745	0.227	17	12.484	0.022

\*From NASA Project SUPER Film Records

**TABLE III-2**  
**DATA TABULATION FOR CASE AI-2**

Shot No.	V <sub>I</sub> , ft/sec	V <sub>I</sub> , km/sec	Target Thickness, in.	Target Thickness, cm	UFS, Measured, ft/sec	UFS, km/sec	P <sub>s</sub> , kb	$\frac{R}{R_0}$	$\frac{P_s}{\rho_0 C_0^2}$
13	24,540	7.481	0.127	0.323	16,205	4.939	582	1.159	0.753
18	26,550	8.094	0.247	0.627	14,155	4.315	484	2.253	0.626
23	24,550	7.484	0.247	0.627	11,751	3.582	377	2.253	0.488
44	23,910	7.289	0.127	0.323	15,488	4.721	547	1.159	0.708
45	24,240	7.389	0.127	0.323	15,034	4.582	525	1.159	0.679
52	25,100	7.651	0.736	1.869	5242	1.598	139	6.715	0.180
55	24,800	7.559	0.736	1.869	5621	1.713	151	6.715	0.195
58	24,800	7.559	1.007	2.558	3613	1.101	91	9.187	0.118
62	24,200	7.376	1.256	3.193	1022	0.311	23	11.459	0.030
63	25,100	7.651	1.253	3.183	1120	0.341	26	11.432	0.033
65	25,100	7.651	1.250	3.175	1020	0.311	23	11.405	0.030
66	24,800	7.559	0.373	0.947	8033	2.449	232	3.403	0.300
67	24,950	7.605	0.373	0.947	9218	2.810	276	3.403	0.357
71	23,600	7.193	0.497	1.262	7512	2.290	214	4.535	0.277
72	23,650	7.209	0.737	1.872	4270	1.302	110	6.724	0.142
323*	25,300	7.712	0.713	1.811	6135	1.870	167	6.505	0.217
324*	25,300	7.712	0.950	2.413	3417	1.042	85	8.667	0.111
327*	25,300	7.712	1.800	4.572	803	0.245	18	16.423	0.024
333*	25,100	7.651	1.420	3.607	944	0.288	22	12.956	0.028
335*	25,300	7.712	0.713	1.811	4542	1.383	118	6.505	0.153
336*	23,500	7.163	0.950	2.413	2988	0.911	73	8.667	0.095
328*	24,600	7.498	1.420	3.607	1098	0.335	25	12.956	0.033

\*From NASA Project SUPER Film Records

TABLE III-3  
DATA TABULATION FOR CASE AI-3

Shot No.	$V_I$ , ft/sec	$V_I$ , km/sec	Target Thickness, in.	Target Thickness, cm	UFS Measured, ft/sec	$U_{FS}$ , km/sec	$P_s$ , kb	$\frac{R}{R_o}$	$\frac{P_s}{\rho_o C_o^2}$
1	15,492	4.722	0.127	0.323	9499	2.895	287	1.640	0.371
2	14,249	4.314	0.127	0.323	7988	2.435	231	1.640	0.300
4	14,459	4.407	0.247	0.627	5859	1.756	174	3.280	0.225
5	13,387	4.385	0.247	0.627	5577	1.700	149	3.280	0.193
7	15,263	4.652	0.495	1.260	2818	0.859	69	6.560	0.089
19	14,039	4.279	0.737	1.870	1727	0.526	41	9.841	0.053
20	15,014	4.576	0.737	1.870	1718	0.524	40	9.841	0.052
25	15,238	4.645	1.000	2.540	1161	0.354	27	13.122	0.035
26	15,381	4.688	1.000	2.540	1155	0.352	26	13.122	0.034
33	13,760	4.194	0.127	0.323	7608	2.319	217	1.640	0.281

**TABLE III-4**  
**DATA TABULATION FOR CASE AI-4**

Shot No.	V <sub>I</sub> , ft/sec	V <sub>I</sub> , km/sec	Target Thickness, in.	Target Thickness, cm	UFS, Measured, ft/sec	UFS, km/sec	P <sub>S</sub> , kb	$\frac{R}{R_0}$	$\frac{P_S}{\rho_0 C_0^2}$
8*	5144	1.567	0.250	0.635	930	0.284	21	6.667	0.027
10*	5085	1.549	0.250	0.635	1190	0.363	27	6.667	0.036
11*	5127	1.562	0.250	0.635	1255	0.383	29	6.667	0.037
17	4992	1.521	0.127	0.323	2030	0.619	48	3.333	0.062
32	5278	1.645	0.063	0.160	3462	1.055	87	1.680	0.112
34	5334	1.626	0.030	0.076	4182	1.275	106	0.800	0.138
35	5208	1.587	0.064	0.163	3737	1.139	94	1.680	0.122

\*Targets were 2024-T4 aluminum alloy.

TABLE III-5  
DATA TABULATION FOR CASE Co-1

Shot No.	$V_I$ , ft/sec	$V_I$ , km/sec	Target Thickness, in.	Target Thickness, cm	UFS Measured, ft/sec	UFS, km/sec	$P_s$ , kb	$\frac{R}{R_0}$	$\frac{P_s}{\rho_0 C_0^2}$
94	18,257	5.565	0.129	0.327	10,360	3.158	888	1.488	0.637
95	19,671	5.996	0.250	0.635	8498	2.590	680	2.884	0.488
96	21,059	6.419	0.250	0.635	9196	2.803	755	2.884	0.542
97*	20,163	6.146	0.501	1.272	4898	1.493	337	5.779	0.242
104*	18,807	5.732	0.719	1.824	3837	1.170	252	8.294	0.181
108*	20,925	6.378	0.501	1.272	4261	1.300	285	5.779	0.204
114*	19,900	6.066	0.912	2.315	2764	0.842	172	10.520	0.123
115*	20,000	6.096	0.910	2.310	3385	1.032	217	10.497	0.156
118*	18,762	6.719	1.133	2.880	1812	0.552	107	13.069	0.077
119	19,900	6.066	0.124	0.315	10,820	3.298	943	1.430	0.676
121	20,800	6.340	0.249	0.632	9967	3.038	842	2.872	0.604
122	21,800	6.645	0.249	0.632	10,099	3.078	858	2.872	0.615

\*Soft copper targets; other targets were hard copper.

**APPENDIX IV**  
**NAVAL ORDNANCE LABORATORY EXPERIMENTAL DATA**

The following data (Table IV-1) are from Fig. 9 of Ref. 23. The projectiles were 0.635-cm-diam (0.25-in.) aluminum spheres. The targets were 7075-0 aluminum plates. The data are plotted in Fig. IV-1.

**TABLE IV-1**  
**NOL DATA**

$V_I$ , ft/sec	$V_I$ , km/sec	Target Thickness, in.	Target Thickness, cm	$P_s$ , kb	$\frac{R}{R_0}$	$\frac{P_s}{\rho_0 C_0^2}$
12,750	3.89	1.50	3.81	6.90	21.45	0.0089
14,150	4.32	1.50	3.81	11.00	20.05	0.0142
16,750	5.11	1.50	3.81	15.50	17.89	0.0200
18,400	5.61	1.50	3.81	18.60	16.79	0.0241
20,300	6.19	1.50	3.81	24.50	15.72	0.0317
25,000	7.62	1.50	3.81	36.00*	13.70	0.0456

\*Extrapolated from Fig. IV-1.

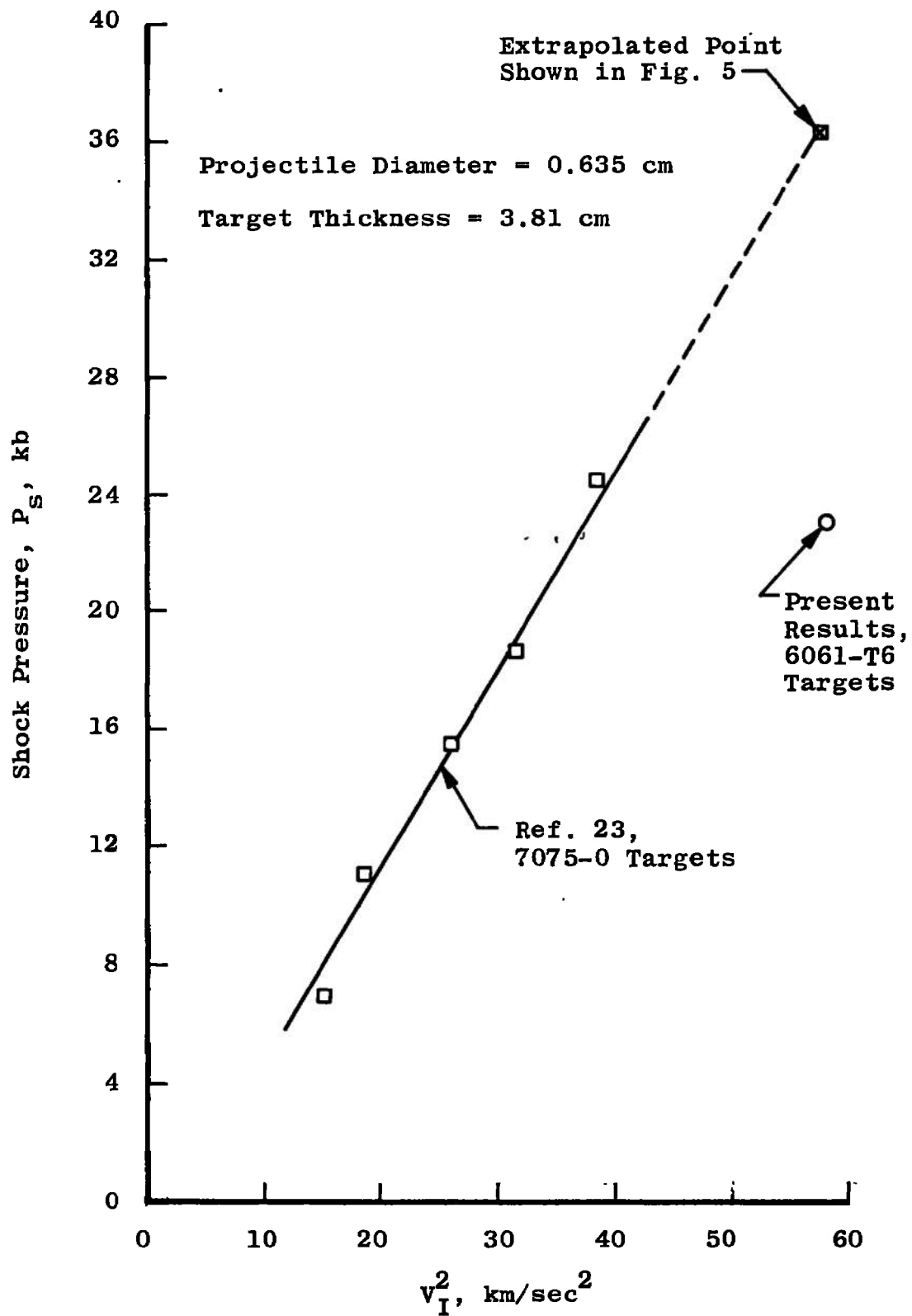


Fig. IV-1 Hypervelocity Impact Shock Pressure Data

# **APPENDIX V** **TARGET MATERIAL YIELD STRENGTH**

The following table contains the yield strength for the various target materials discussed in this report.

<u>Target Material</u>	<u>Yield Strength, psi</u>	<u>Reference</u>
1100-0	5,000	30
2024-0	14,000	30
2024-T4	40,000	30
7075-0	18,000	23
6061-T6	40,000 (2-percent Offset)	31
Hard Copper*	43,000 (2-percent Offset)	31
Soft Copper*	12,800 (2-percent Offset)	31

---

\*Hard rolled high purity copper plates were used for targets less than 1.27 cm thick. Soft high purity copper was used for the thick targets.

UNCLASSIFIED

Security Classification

## DOCUMENT CONTROL DATA - R &amp; D

(Security classification of title, body of abstract and indexing annotation must be entered when the overall report is classified)

1. ORIGINATING ACTIVITY (Corporate author) Arnold Engineering Development Center ARO, Inc., Operating Contractor Arnold Air Force Station, Tennessee		2a. REPORT SECURITY CLASSIFICATION UNCLASSIFIED	
		2b. GROUP N/A	
3. REPORT TITLE COMPARISON OF EXPERIMENTAL AND PREDICTED AXIAL PRESSURE VARIATION FOR METALLIC TARGETS IMPACTED BY METALLIC SPHERES			
4. DESCRIPTIVE NOTES (Type of report and inclusive dates) November 27, 1967 to June 30, 1968 - Final Report			
5. AUTHOR(S) (First name, middle initial, last name)  James P. Billingsley, ARO, Inc.			
6. REPORT DATE July 1969		7a. TOTAL NO. OF PAGES 57	7b. NO. OF REFS 31
8a. CONTRACT OR GRANT NO. F40600-69-C-0001		9a. ORIGINATOR'S REPORT NUMBER(S)  AEDC-TR-69-49	
b. Program Element 65401F			
c.		9b. OTHER REPORT NO(S) (Any other numbers that may be assigned this report)	
d.		N/A	
10. DISTRIBUTION STATEMENT  This document has been approved for public release and sale; its distribution is unlimited.			
11. SUPPLEMENTARY NOTES  Available in DDC.		12. SPONSORING MILITARY ACTIVITY Arnold Engineering Development Center Arnold AF Station, Tennessee 37389	
13. ABSTRACT  Sufficient experimental data have been collected for five different cases of high velocity metallic impact so that the axial shock pressure variation can be traced in a semi-infinite target. The metals utilized were aluminum alloys and copper. In all cases, a spherical projectile was fired into a target plate of similar material. The aft spall velocity of the target plate was measured by means of a high-speed framing camera, and the shock pressure at the axial location in a semi-infinite target corresponding to the target plate thickness was computed from this spall velocity. These data are compared with the results of various theoretical methods for predicting the shock pressure variation in semi-infinite targets. The present data are also compared with other available experimental data.			

14.

## KEY WORDS

## LINK A

## LINK B

## LINK C

ROLE

WT

ROLE

WT

ROLE

WT

pressure

copper

aluminum alloys

targets

hypervelocity projectiles

spheres

impact tests

impact shock

hypervelocity impact

impact theory

1. Targets -- Spalling

2 " -- Impact pressures

3 Spheres -- Impacting

4 " -- Impact pressure

5 Impact theory -

1 - 2